Integrated optical networks of microring resonators

a comparison between theory and experiment

Tutor: MSc. C. Taballione

Teacher: Prof. Dr. K.J. Boller

UNIVERSITY OF TWENTE

BACHELOR ASSIGNMENT

H.K. Volbeda

May 4, 2016

List of Figures

Contents

Introduction

For every application, specialized filters need to be designed to fit the needs and purpose of the application. In the designing process there is an almost endless list of posibilities, but in practice the design of the chip is limited to the scale and complexity of the geometry for the manufacturer. Within the manufacturing process there are a certain set of aspects that can have an dimensional error in them. The height of an waveguide can be grown in near atom-like precision. An error of one nanometer in the height will not alter the way the optical filter behaves, but the geometry of a waveguide in the planar direction is much more susceptable to error. In the thickness of the waveguide the error of fabrication can be about 10 nm, or around 10 atomic layers in the deposition process of fabrication. In the width is around 50 nm, which is almost comparable with the width of the waveguide. That is why the error in width is of more significance for it affects the performances of the waveguide negatively making it absolutely nescessary to understand if the filter on the chip one designed has the same dimensions as the end product recieved. The error of fabrication in the cross-section can give complications for the geometry of the waveguide structure: the optical filter. By analysing geometry and transmission spectra of an optical filter, fabrication errors can be revealed. By combining the mathematical theory of System Transfer Functions in the Z-domain, incorporating all variables of the filter into one formula relating input to output and with a fitting procedure one can extract the characterising coefficients needed to compare the designed with the received filter.

In the following report, the description of two different optical filters will be presented, to show the use of digital filter theory on optical filters. Starting with a theoretical chapter explaining the working of a specific optical filter, an optical waveguide ring resonator and its performance. In the next chapter the Z-Transform and the system transfer function will be explained followed by a two chapters on visualising the system transfer function, rewriting it into a fitting model and the workings of the fitting procedure. The chapters following will discuss the setup of measuring and the results of those measurements. The last chapter will conclude the experiments explained in previous chapters.

Chapter 1

Ring Resonator Devices as Optical Filters

Any optical filter can be summarised to a simple principle: an EM wave sent into an optical filtering device, altered by a filter whereupon the altered EM wave leaves the device. This situation can be used in two different ways.
Firstly, the input- and the outputsignal of the optical filter are known but the internal composition of the filter is unknown. Secondly, the internal filter network is known but the spectral filtering is still to be determined. The two different ways can be used together to compute the behaviour of a complex optical filter.
Designing an optical filter is done by combining small individual filter components that have a known internal composition because they are the building blocks of a larger filter network. By reverse engineering a large optical filtering network, for example consisting of microring resonators, can be decomposed into the small buildingblocks mentioned above and knowing its key characterization points, such as the Free Spectral Range and the Finesse, is needed for full understanding of a large network.

1.1 The base of an optical filter, the simplest case

A large optical filter is constructed of multiple elements where a frequently used and conviniently the most simple, element in optical filter networks is the single all pass ring resonator. This device will be briefly explained in this section, see figure 1.1, and explained in detail further along this report.

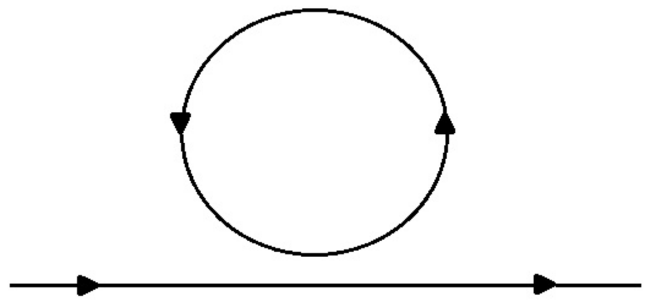

Figure 1.1: Simple representation of a single ring resonator

Any microring resonator consists of one or multiple looped waveguides and one or multiple straight waveguides. The term ring indicates a closed loop of any shape, for example a NASCAR racetrack shape (elongated circle) but for convienience all rings will be circular. When an, in the time domain infinitely short, electromagnetic pulse is injected from the left of figure 1.1 it travels into the coupling region. The coupling region is the section of figure 1.1 where the looped ring and the straight waveguide are nearest to each other. At the coupling region the light partially cross couples into the ring from straight waveguide to looped waveguide, travels around the loop, partially cross couples out of the ring to finally be redirected to exit at the right. Only if the optical path length of the looped waveguide has an optical length equal to an integer amount of the wavelength of the injected signal, are the waves from the looped waveguide and the bus waveguide able to interfere destructively achieving an output of zero power. This destructive interference is called resonance and is given in the form of an equation below:

$$L_{optical} = n\lambda_{injected} \tag{1.1.1}$$

Looking at this resonance condition it is clear to see that a ring resonator can support multiple resonances.

1.2 Spectral Filtering, Input vs Output

To show what a ring resonator device in figure 1.1 does with an incoming signal one needs to consider what the transmission of the ring resonator is for a single sample of a continuous signal. Figure 1.2 shows the output of the ring resonator in the time domain when only a single sample as input is taken. The response shown is observed periodically at certain interval times that match the time it takes for the signal to travel the optical length of the looped resonator.

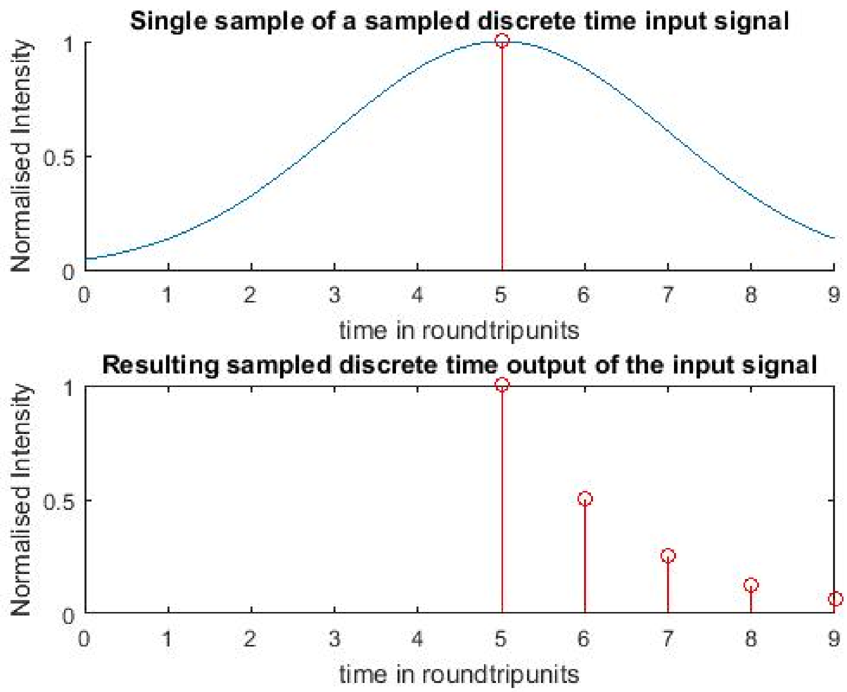

Figure 1.2: Schematic of the input and output of a single ring resonator time for the case that an input is an ultra-short delta function like pulse that represents a part of a continuously varying input. The round trip loss is equal to 50%.

When a high pulse, resembling the input signal in graph 1.2, is send through aan all pass ring resonator, the light will pass through the straight bus waveguide and end up at the output after a certain travel time. When the light passes the coupling region it will partially cross couple into the ring, make one roundtrip, again partially cross couple out to travel to the output. The total power is dependent on the rate of decay per roundtrip inside the ring and the coupling coefficient into and out of the ring. Light inside the ring can travel another roundtrip before coupling out and end up at the output as a second echo separated by the first one due to the roundtrip time. The first sample of the output signal shows a complete transmission of the incoming sample, but the second sample, taken one time unit later, shows a much lower transmission and a third sample, taken two time units later than the first sample, shows an even lower transmission.
In summary, a single ultrashort sample of a continuous input generates a series of temporally equidistant transmission echo's at the output. The rate of decay from one echo to the next is given by the power loss coefficient r. As an example, if the power from echo to echo is 50% one obtains an exponential decay of all echo's with a half-power lifetime of one roundtrip time. An optical filter can be created with any value for the power loss in the waveguides, but if the filter is to be used in a wide range of applications a power loss rate of 10% or less seems physically appropriate[1].

In order to predict the transmission for a signal that is continuously varying, the continuous signal must be approximated by sampling; a sufficiently dense series of samples are taken periodically in time. By using a superposition of all echoes of all these samples it becomes possible to determine the periodically sampled estimation of the output signal. Imagine an incoming signal consisting of several samples where each single sample has the response as explained at figure 1.2, this describes the complexity of ring resonators when looked at in the time domain.

1.3 Characterization through Free Spectral Range, Finesse and ring radius

As an example the transmission spectrum of the single all pass ring resonator of figure 1.1 is shown in figure 1.3

1.3.1 Free Spectral Range

The wavelength spacing between neighbouring resonances is called the free spectral range (FSR) and depends on the wavelength of resonance (λ_{res}) [2], the refractive index (n) and the geometrical length of the loop waveguide ($L_{geometrical}$) [3],

$$\mathrm{FSR} = \frac{\lambda_{res}^2}{n \cdot L_{geometrical}} \tag{1.3.1}$$

A wide FSR can be accomplished by reducing the curvature of the looped waveguide, making the optical path length smaller. Another way to widen the FSR by lowering the refractive index of the looped waveguide, so the optical path decreases. Please recall that when in resonance, the light from the looped waveguide interferes destructively with the light from the straight bus waveguide. When in destructive interference the intensity at the output is at a minimum, the wavelengths corresponding to a minimum power are called resonance wavelengths. The filter characteristics seen in figure 1.3 are those of a notch filter.

1.3.2 Finesse

Another factor to describe the behavior of a ring resonator circuit is the Finesse (F) which is a measure of the sharpness of the resonance relative to the spacing of the resonances; the ratio of the FSR and the full-width of the large dip in the transmission spectrum at half-maximum (FWHM). In terms of energy the Finesse is dependent on the amount of stored energy in the filter divided by the amount of energy lost by the signal travelling the optical length of the looped waveguide. The Finesse is given by the following formula:

$$F = \frac{\mathrm{FSR}}{\mathrm{FWHM}} \tag{1.3.2}$$

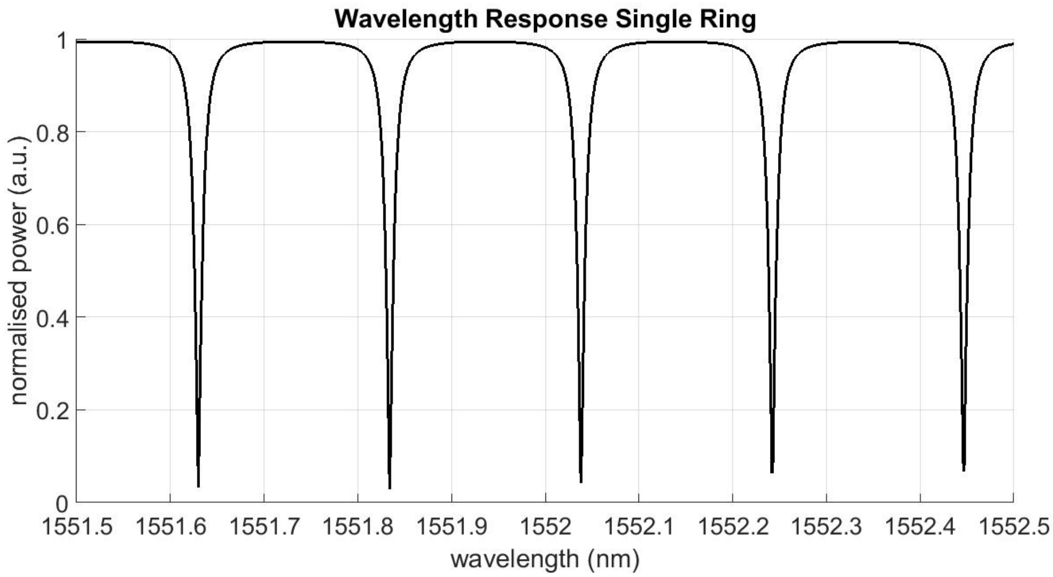

Figure 1.3: Notch filter characteristic of a single ring resonator. Modelled with a power loss of 10%, a cross coupling percentage of 20%.

A device with a high Finesse has a small FWHM and a strong intensity build-up in the ring when in resonance; the loss of power inside the looped waveguide is low, therefore the enhancement of intensity is high. This can likewise be seen in the transmission spectrum of a device, as a high Finesse shows sharper peaks and a lower transmission maxima than a low Finesse device.

1.3.3 Characterisation of the ring radius

When evaluating a transmission spectrum of a ring, the FSR is almost never calculated by formula 1.3.1. Instead the opposite is done, the radius R and geometrical length $L_{geometrical}$ are calculated from the FSR which can be found from the transmission spectrum, using the resonance wavelengths and the group refraction index of the material the ring is made from. The geometrical length, optical length and the radius of the ring resonator can be calculated from the FSR and the resonance wavelengths. The optical length of the ring resonator $L_{optical}$ is equal to two pi times the radius of the ring R times the group refraction index n.

$$L_{optical} = 2\pi R \cdot n_{group} \tag{1.3.3}$$

The calculation of the optical length of the ring is not obvious as the radius of the ring is the unkown variable but the following formula can be recalled at resonance.

$$L_{optical} = m \cdot \lambda_m \tag{1.3.4}$$

Where m is an integer and λ_m is the corresponding resonance wavelength. Using two consecutive peaks of a transmission spectrum, for example figure 1.3, the following mathematical calculation can be done:

$$L_{optical} = m \cdot \lambda_m = (m+1) \cdot \lambda_{m+1} \tag{1.3.5}$$

Which results in m being equal to $\frac{\lambda_{m+1}}{\lambda_m - \lambda_{m+1}}$. The optical length of the ring resonator can be calculated using two consecutive resonance wavelengths, which is essentially the FSR of the figure. In the following equation formula 1.3.1 is rewritten to:

$$L_{optical} = \frac{\lambda_r^2}{\mathrm{FSR}} \tag{1.3.6}$$

The radius of the ring resonator R is then calculated by use of the optical length and the group index n to the last formula of this section:

$$R = \frac{\lambda_r^2}{2\pi n_{group}\mathrm{FSR}} \tag{1.3.7}$$

To be able to caracterise a ring resonator which has not been measured yet a mathematical modelling approach can be used to get a transmission spectrum of the ring resonator. In the following chapters the several approaches are explained and discussed.

Chapter 2

Fourier Transform, Laplace Transform and Z-Transform

There are several mathematical approaches that can be used to characterize or design an optical filter consisting of microring resonators: the Fourier Transform, the Laplace Transform and the Z-Transform. Which transform is to be used with an optical filter depends entirely on convenience or if an alternate insight is required.

2.1 Fourier Transform and Laplace Transform

The Fourier Transform is preferably used when the input signal and the output signal of a filter are continuous. The Fourier Transform is shown in equation 2.1.1 which describes a transformation of a signal $f(t)$ from the time domain to the frequency domain.

$$F(\omega) = \frac{1}{2\pi}\int_{-\infty}^{\infty} f(t)e^{-i\omega t}dt \tag{2.1.1}$$

The Laplace Transform of a time dependent function $f(t)$ is used with transient signals where a transient signal is regarded as a sudden change in a signal.

$$F(s) = \int_{0}^{\infty} f(t)e^{-st}dt \tag{2.1.2}$$

When a transient signal is send through a filter, the resulting output signal is in like manner transient. Expressing undefined terms in a continuous signal using the Fourier Transform requires using an infinite summation over all sinusoids, instead of a finite number for expressing a time-periodic signal as stated with Laplace. As an infinite sum of sinusoids is impractical, the Laplace Transform is more convenient. A transient signal can still be continuous as the duration of the disruption in the signal can extend over several units of time; a disruption of the signal does not have to be infinitely short. Would the transient signal include infinitely short disruptions of the discrete time counterpart, as shown by the example made in figure 1.2, another form of the Laplace Transform can be used: the Z-Transform.

2.2 Z-Transform

The Z-Transform is the discrete time counterpart of the Laplace Transform and is therefore derivable from the Laplace Transform. Starting from expression 2.1.2, the Z-Transform can be derived by sampling the continuous-time input signal $f(t)$ at m instances in time that are separated by the sampling time interval, T_s. For the sampled signal $f(m)$, with m an integer, assuming the sampling period to be normalized and dimensionless for simplicity, T_s=1, the Laplace Transform becomes:

$$F(e^s) = \sum_{m=0}^{\infty} f(m)e^{-sm} \tag{2.2.1}$$

From the definition of Laplace it is known that $s = \sigma + i\omega$ is the complex frequency with σ and ω being real numbers. When substituting e^s for z in equation 2.2.1, one obtains the final form of the Z-Transform as:

$$F(z) = \sum_{m=0}^{\infty} f(m)z^{-m} \tag{2.2.2}$$

The Z-Transform was derived from the Laplace Transform, but there is additionally a close relation to the Fourier Transform. The basis function of the Z-Transform can be expanded into the following form[5]:

$$z^{-m} = (e^{\sigma}e^{i\omega})^{-m} = r^{-m}e^{-i2\pi fm} \tag{2.2.3}$$

The relation $\omega = 2\pi f$ was used. The variable r is the rate of decay of the amplitude of a complex sinusoid, of which the influence on the basis function z can be seen in figure 2.1.

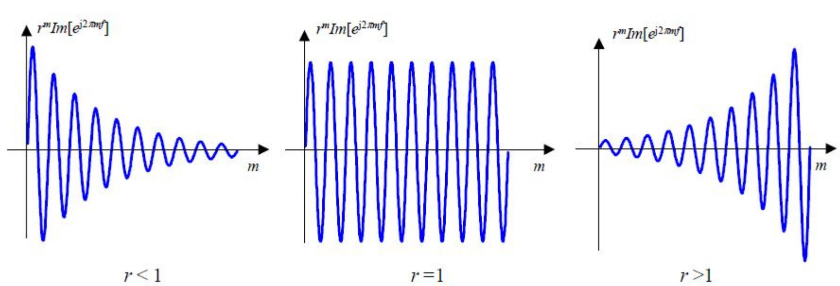

Figure 2.1: Basisfunctions of the Z-Transform [5]

The expression $z^{-m} = r^{-m}e^{-i2\pi fm}$ converts to the basis function of the Fourier Transform in the case of $r = e^{\sigma} = 1$ (see the middle of the figure) which is complex exponential with a time-invariant amplitude and phase. However the Fourier Transform functions ($r = 1$) are less suitable for transient time signals. The basic functions for the Z-Transform are damped or growing sinusoids, which are visualized by the outer two pictures in figure 2.1. The variable r describes the power loss per roundtrip through the looped waveguide. The power loss can be taken outside the basis function, resulting in the following:

$$F(z) = \sum_{m=0}^{\infty} f(m)r^{m}z^{-m}, \tag{2.2.4}$$

Where $f(m)$ is the discrete time signal while the original (not-sampled) transient signal is $f(t)$. r^m is the power loss of the signal after m roundtrips through the ring resonator circuit and z^{-m} is the basis function of the Z-Transform per roundtrip through the ring resonator circuit. Mathematically, a finite power loss (r<1) ensures that the sum is convergent. If r would be bigger than 1, such as for amplification of light in each roundtrip, the sum would be divergent, giving an exponentially increasing output signal. The only physically acceptable basis function of the Z-Transform is the decaying oscillation in figure 2.1

2.3 System Transfer Function

A Z-Transform formula for characterising signals in the discrete time domain was derived, but how does it make describing a microring structure any easier?
By rewriting the Z-Transform in a form that relates the input signal to the output signal it is possible to characterize a microring resonator network with one compact expression. In the beginning of this chapter it was stated that there is an incoming signal into the ring resonator of figure 1.1 and an outgoing signal. The input signal is causal and has impulse response $x(n)$. The output has impulse response $y(n)$ in the discrete time domain. Converting the input signal in the discrete time domain to the Z-domain by using the Z-Transform is represented by:

$$X(z) = x[0] + x[1]r^{1}z^{-1} + x[2]r^{2}z^{-2} + \cdots = \sum_{n=0}^{\infty} x[n]r^{n}z^{-n} \tag{2.3.1}$$

Calculating the Z-Transform of an output signal is in mathematical form the same as with the input signal:

$$Y(z) = y[0] + y[1]r^{1}z^{-1} + y[2]r^{2}z^{-2} + \cdots = \sum_{n=0}^{\infty} y[n]r^{n}z^{-n} \tag{2.3.2}$$

Without more knowledge about $x[n]$ and $y[n]$ it is not possible to further simplify these expressions.

The Z-Transform follows, much like the Fourier Transform and the Laplace Transform, a convolution rule. For two input signals in the discrete time domain, $x_1[n]$ and $x_2[n]$, it can be proven that the convolution of the two signals in the discrete time domain is the same as multiplication of the two signals in the Z-domain [5]:

$$x_1[n] \otimes x_2[n] \Longleftrightarrow X_1 \cdot X_2 \tag{2.3.3}$$

This relation will be used for the further explanation of a system transfer function.

For future reference, it is possible to simplify $\sum_{n=0}^{\infty} r^n z^{-n}$, in the case of $x[n]$ or $y[n] = 1$ by using the following power law:

$$\sum_{n=0}^{\infty} a^n = \frac{1 - a^{n+1}}{1 - a}, \tag{2.3.4}$$

Where a is taken to be $a = rz^{-1}$. This power law will simplify further when $|a| < 1$:

$$\sum_{n=0}^{\infty} a^n = \frac{1}{1 - a} \tag{2.3.5}$$

This equation is used extensively because it is a way of simplification; expressing signals as infinite sums, especially when the input and the output impulse response $x[n]$ and $y[n]$ exhibit the same type of infinite sums.

The impulse response $y[n]$ is the convolution of the systems impulse response and the input impulse response.

$$y[n] = h[n] \otimes x[n] \Longrightarrow Y(z) = H(z)X(z) \Longrightarrow H(z) = \frac{\sum_{n=0}^{\infty} y[n] r^n z^{-n}}{\sum_{n=0}^{\infty} x[n] r^n z^{-n}} \tag{2.3.6}$$

By dividing the Z-Transform of the output signal by the Z-Transform of the input signal the System Transfer Function is revealed.

Chapter 3

Characterising simple ring resonator circuits

In the following chapter, two different simple waveguide ring resonators circuits are evaluated using the Z-Transform: The single all pass ring resonator and the single add drop ring resonator. These two circuits are frequently used in more complex waveguide ring resonator networks.

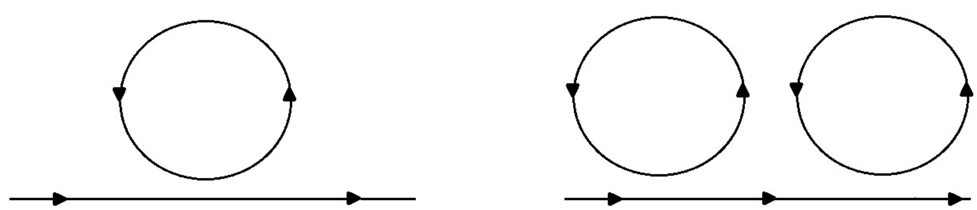

(a) Single All Pass ring resonator (b) Double All Pass ring resonator

Figure 3.1: Overview of discussed Ring Resonator Devices

3.1 The Single All Pass ring resonator

As showed in chapter 2 the single all pass ring resonator, see figure 3.1a and shown more detailed in figure 3.2, consists of a straight bus waveguide and a single ring resonator. When calculating the system transfer function of these circuit it is necessary to have an orderly system, therefore some simplifications and assumptions are required.

By assuming there are no internal reflections back to the input port it can be said that all signals travel in only a single direction, from the input port to the output port as indicated by the arrows. Furthermore, the power exchange between the ring resonator and the straight bus waveguides only takes place in the coupling region, marked in figure 3.2 by the two crossing arrows.

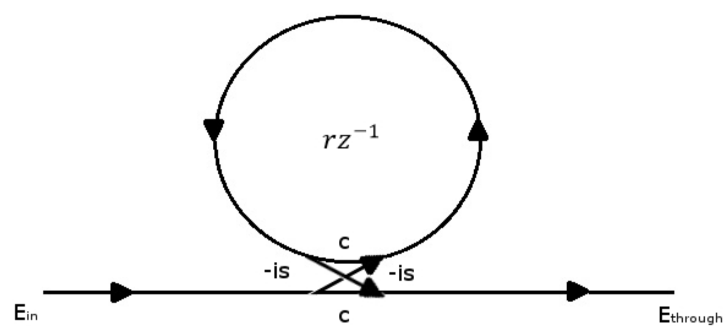

Figure 3.2: The single All Pass ring resonator. The arrows describe the signal flow inside the system.

Figure 3.2 shows a signal E_{in}, which is a signal composed of a traveling light wave coming from the left and an output signal $E_{through}$ exiting the system. The constant $c \in C$ is called the self-coupling coefficient and it describes the amount of light inside the bus waveguide or the ring resonator. The constant $s \in C$ is the cross coupling coefficient and it describes the coupling losses across the coupling region, marked by the crossing arrows. Looking back at section 2.3, the fractional power loss inside the ring resonator is $(1 - r)$ and one of the basic functions of the Z-Transform is z^{-1}, coming from z^{-m} where $m = 1$ for one roundtrip along the looped waveguide.
By assuming there are no losses in the coupling region, marked by the two crossing arrows, the following can be stated [4]:

$$s^2 + c^2 = 1 \tag{3.1.1}$$

Within the ring resonator system coupling takes place at the coupling regions, marked by the crossing arrows, but due to repeated roundtrips the amount of coupling can greatly influence the strength of the output signal. Three kinds of situations can be stated, undercoupling, critical coupling and overcoupling.
When the power loss inside the ring resonator is smaller than the amount of light that couples into the ring, $(r < s)$ it is called undercoupling. The buildup of light inside the ring resonator occurs with a lag of the phase compared to the light travelling through the straight waveguide, there is a partial destructive interference, leaving at the resonance partial destructive interference.
At critical coupling the power loss per roundtrip is the same as the amount of light coupling into the ring, $(r = s)$. The buildup of light inside the ring resonator becomes equal to the power that bypasses the ring directly such that the destructive interference

at the output port becomes complete.
The third and last kind of coupling is overcoupling, which occurs when the power loss is larger than the amount of light coupling into the ring, ($r > s$), leaving a large amount of light leaving the ring resonator with a phase difference which results in a partial destructive interference, leaving an output signal which is larger than zero at resonance. When injecting a non-resonant signal, there is no power-buildup inside the resonator such that all light is bypassed; there is full signal at the output off-resonance.
The scenario of critical coupling is the desired one, as any other scenario would result in a low yield leaving an imperfect resonance system. In the case of critical coupling full incoming power is coupled into the all pass ring resonator thereby providing a perfect notch filter characteristic as displayed in figure 1.3. The case of critical coupling (or subsequently called impedance matching) is important for making a larger filter network consisting of single ring resonators.
In formula 2.3.6, the signal transfer function is defined as:

$$H(z) = \frac{\sum_{n=0}^{\infty} Output}{\sum_{n=0}^{\infty} Input} \tag{3.1.2}$$

Depending on the degree of complexity of the system, meaning if the system has multiple outputs, multiple inputs or a cascading design of rings, the derivation of the system transfer function can be mathematically extremely challenging. The single waveguide resonator is considered a simple system, making it possible to perform a straightforward calculation. By summing all the different ways (paths) the signal can travel through the system, starting with the path spanning the least optical distance and ending at the longest path, the system transfer function can be calculated.

- Path number 1: The light travels through the straight bus waveguide without cross coupling into the ring resonator.

$$E_{through} = cE_{in} \tag{3.1.3}$$

- Path number 2: The light cross couples into the ring resonator and goes *once* around the loop to exit the loop again and travel through the straight bus waveguide.

$$E_{through} = [(-is)rz^{-1}(-is)]E_{in} \tag{3.1.4}$$

- Path number 3: The light cross couples into the ring resonator and goes *twice* around the loop, without cross coupling to the straight bus waveguide after one loop.

$$E_{through} = [(-is)(rz^{-1})c(rz^{-1})(-is)]E_{in} \tag{3.1.5}$$

- Path number 4: The light cross couples into the ring resonator and goes *three* times around the loop. Again it only cross couples after 3 times around the ring resonator.

$$E_{through} = [(-is)(rz^{-1})c(rz^{-1})c(rz^{-1})(-is)]E_{in} \tag{3.1.6}$$

The mathematical form of all subsequent paths, can be derived from the structure of equations 3.1.4 till 3.1.6. With taking all paths into account, the system transfer function assumes the following form:

$$\begin{aligned} H(z) &= \frac{\sum E_{through}}{E_{in}} \\ &= \frac{cE_{in} + (-is)^2 rz^{-1}E_{in} + (-is)^2(rz^{-1})^2 cE_{in} + (-is)^2(rz^{-1})^3 c^2 E_{in} + \dots}{E_{in}} \end{aligned} \tag{3.1.7}$$

When dividing the $\sum E_{through}$ by E_{in}, the system transfer function can be rewritten in the following way:

$$\begin{aligned} H(z) &= c + (-is)^2 rz^{-1} + (-is)^2(rz^{-1})^2 c + (-is)^2(rz^{-1})^3 c^2 + \dots \\ &= c - s^2 rz^{-1}[1 + crz^{-1} + (crz^{-1})^2 + \dots] \end{aligned} \tag{3.1.8}$$

To simplify the expression for $H(z)$ the following power series is used, $\sum_{n=0}^{\infty} x^n = \frac{1-x^{n+1}}{1-x}$, with the abbreviation $x = crz^{-1}$. Since $|x| < 1$, as c and r are both smaller than one, the power series converges to $\sum_{n=0}^{\infty} x^n = \frac{1}{1-x}$, thereby yielding a strongly shortened expression for H(z):

$$H(z) = c - s^2 rz^{-1}[\frac{1}{1-crz^{-1}}] = c[\frac{1-crz^{-1}}{1-crz^{-1}}] - \frac{s^2 rz^{-1}}{1-crz^{-1}} = \frac{c - c^2 rz^{-1} - s^2 rz^{-1}}{1-crz^{-1}} \tag{3.1.9}$$

When losses are absent in the coupling region, equation 3.1.1 is valid. The system transfer function of a single all pass ring resonator assumes a rather simple form[7]:

$$H(z) = \frac{c - rz^{-1}}{1-crz^{-1}} \tag{3.1.10}$$

3.2 The Double All Pass ring resonator

The single ring resonator is a simple system, but it is not the only possible configuration of the all pass single ring resonator. A huge variety of transfer systems with additional ring resonators is possible. A most simple example for such a network is shown in figure 3.1b where two all pass resonators are coupled in series. In general serially coupled single ring resonators introduce a new system that can generate an entirely different impulse response than a single ring resonator.

Examining the double all pass ring resonator will show how the output of a single all pass ring resonator changes when put in series with more single ring resonators.

Before determining every possible path the input signal can take before ending up at the output, it is important to look at the convolution property of the Z-Transform again.

From section 2.3 it is recalled that the convolution of two signals in the time domain is the same as the multiplication of the two signals in the Z-domain.

$$X_1(n) \otimes X_2(n) \Longleftrightarrow H_1 \cdot H_2 \tag{3.2.1}$$

Two resonators are placed in series, the output of the first forming the exclusive input to the second one. While each resonator performs a convolution in the time domain, it is allowed to say that the system transfer function of a double all pass ring resonator is the same as a multiplication of the system transfer functions of the independent ring resonators. But before the convolution is applied, let us look at the double ring system.

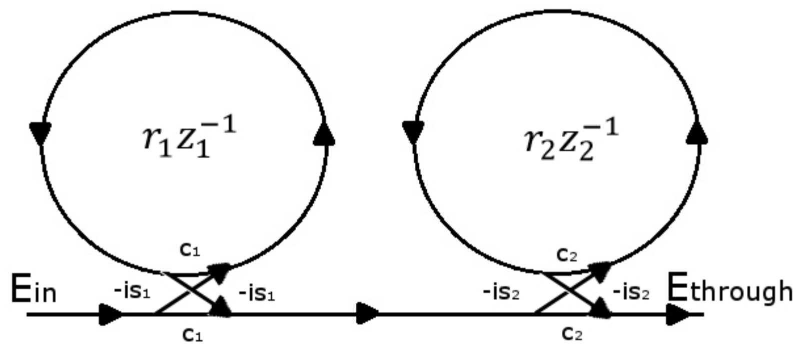

Figure 3.3: The double all pass ring resonator.

A signal E_{in} is entering from the left, travelling through the system and exiting the system at the right of the figure. The constants $c_1, c_2 \in C$ are again the self-coupling coefficients and the constants $s_1, s_2 \in C$ are the cross coupling coefficients. The loss of power inside ring resonator 1 and 2 are given via r_1 and r_2. z^{-1} is the first basis function of the Z-Transform.
The total system transfer function including the convolution rule can be stated in the following manner:

$$H_{total} = H_{ring1} H_{ring2} \tag{3.2.2}$$

The system transfer function of one ring was already calculated in the last section $H(z) = \frac{c - rz^{-1}}{1 - crz^{-1}}$. By substituting r with r_1 and r_2 and substituting c with c_1 and c_2 gives the following total transfer function:

$$H(z) = [\frac{c_1 - r_1 z^{-1}}{1 - c_1 r_1 z^{-1}}][\frac{c_2 - r_2 z^{-1}}{1 - c_2 r_2 z^{-1}}] \tag{3.2.3}$$

The evaluated system might seem simple again, but keep in mind that summing up the partial signals of all possible paths would be very tedious and much less straight forward than in equations 3.1.4-3.1.6 and equation 3.1.10. The reason being that the output of the first ring resonator is the input of the second ring resonator. This means that every repetition the first ring output signal is further distorted after traveling through the second ring resonator, making the signal at $E_{through}$ more difficult than what was presented in figure 1.2. A combined transmission spectrum of a double all pass ring resonator system is represented in figure 3.4. To show more clearly the characteristics of a double all pass ring resonator system the second ring has been chosen as 1.5-times larger than that of the first ring.

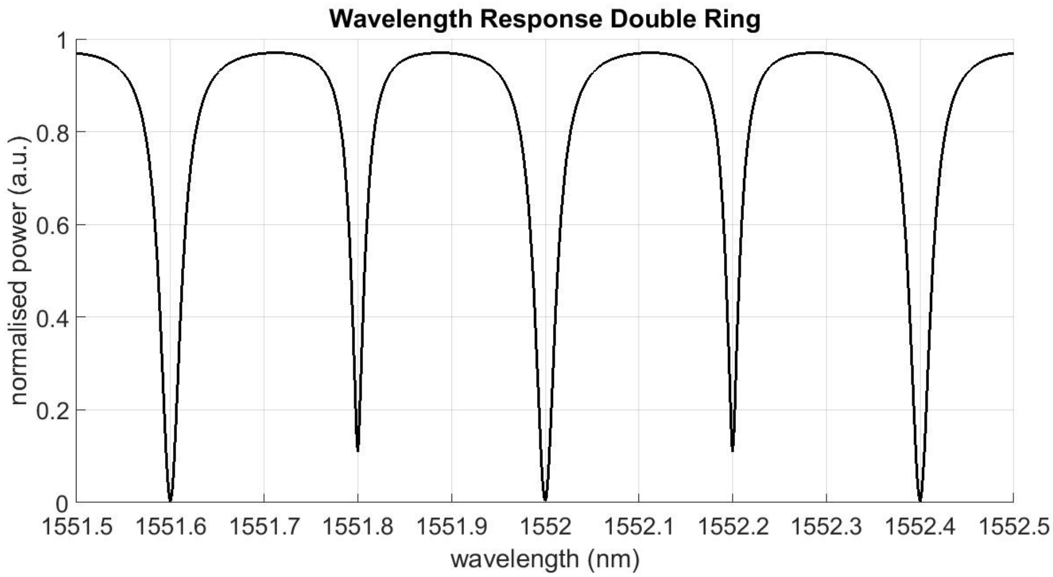

Figure 3.4: The Notch Filter characteristics of a double all pass ring resonator system at critical coupling. The wavelength response graph was modulated with $r_1 = 10\%$, $r_2 = 20\%$, $s_1 = 20\%$ and $s_2 = 30\%$.

From this graph can be extracted that the second ring, with a larger radius, has a 1.5 times smaller Free Spectral Range than the first ring. Would both rings have the same radius, the Free Spectral Ranges of the first and second ring would overlap, leaving no difference between the two leaving the system in matched resonance. The Finesse of this so called second order ring resonator system can be calculated from a combined FSR which is the lowest common multiple of the two individual FSRs of the ring resonators.

Characterising a ring resonator using a mathematical system transfer function. This system transfer function can be used in two different ways. Firstly to give an estimation or prediction of a ring when the coupling coefficients and the powerloss coefficient are given. Secondly to evaluate a transmission spectrum with unkown coupling coefficients and an unknown powerloss coefficient. The second approach is used extensively to analyse transmission spectra of devices with known geometry to verify the designed dimensions of the waveguides.

Chapter 4

Z-transform Modelling

A visualisation where multiple variables can be altered and predictions can be made without measuring is called a model. For the following model the software MATLAB was used.

4.1 From the z-domain to the frequency domain

To modulate the transfer function the model and comparing tool it must be dependent on wavelength or frequency, the basis function z^{-1} must be rewritten.

$$z^{-1} = e^{-i\omega} \tag{4.1.1}$$

Here ω is the frequency, or in units Hz.

4.2 Model Parameters

With every model, there are parameters to be taken into account. There are the obvious parameters that show directly from the transfer function; c and r. The value of the self coupling coefficient c is between 0 and 1, 0 corresponds to 0% self coupling and 1 to 100% self coupling. The round trip power loss has the same domain, but 0 corresponds to 0% transmission of power per roundtrip and 1 corresponds to 100% transmission of power per roundtrip.
With parameters c and r properly defined, the less obvious parameters are to be explained. The new basis function $e^{-i\omega}$ can model the period of the function. The period must be possible to alter as, it is directly linked to the FSR describing the period of a transmission function. This is done by multiplying the exponent with the parameter L. Where L is in units of one over wavelength.

$$z^{-1} = e^{-2\pi i\omega L} \tag{4.2.1}$$

Now a single ring resonator can be modelled using optical parameters c, r and L. For a double all pass ring resonator the amount of parameters needed are a total of six as each c, r and L are ring specific.

4.3 The complete model function

The final stage of completing the model is getting rid of the imaginary component in the exponent to visualise the model in the real domain instead of the imarinary domain. By multiplying the whole transferfunction with its complex conjucate, a well known mathematical trick, the imaginairy components can be rewritten into a combination of sine and cosine.
To summarise: The system transfer function $H(z) = \frac{c-rz^{-1}}{1-crz^{-1}}$ can be rewritten to the following form:

$$|H(\omega)| = |\frac{c - re^{-2\pi i\omega L}}{1 - cre^{-2\pi i\omega L}}| = \sqrt{\frac{c^2 - 2crcos(\pi L(\omega + b)) + r^2}{1 - 2crcos(\pi L(\omega + b)) + c^2r^2}} \tag{4.3.1}$$

Where the following parameters are important:

- Self coupling coefficient c ranges from 0 to 1, unitless
- Round trip loss r ranges from 0 to 1, unitless
- Period L, in units of $[\lambda^{-1}]$

The model described is suited for the single all pass ring resonator, the least difficult case, and a good example of how to use a z-transform to visualise a system that has not been measured yet. Predictions can be made by inserting values of c, r and L.

Instead of using the model as a discovering tool it can, and will be extensively used as a data analysis tool. When fitting the model to experimental data, the parameters c, r and L of the model can be computationally altered to fit the data therefore aproximating the values of c, r and FSR of the actual system. This last mentioned way of working will be used to process results where more parameters will be added. The parameters added are not as fundamental as the parameters mentioned above. They are merely to facilitate MATLAB in finding the best fit of the model with the provided data of the results.

Chapter 5

Model Fitting using MATLAB Curve Fitting Tool

To fit the z-transform model described in the previous section, an extention of MATLAB was used: the curve fitting tool (cftool). This toolbox uses several variations on the method of least squares when fitting data, relating a model to a specified dataset with one or more coefficients.

5.1 Goodness of Fit Satistics

5.1.1 Sum of Square Error

In the process of obtaining the best estimate of the models coefficients, cftool minimizes the summed square of residuals, or Sum of Square Errors (SSE)[11]. This error, or residual, is defined as the difference between the value of a previously specified datapoint and the corresponding modelled datapoint. The error for the ith datapoint is r_i, the value of the specified datapoint y_i and the value of the fitted datapoint $\hat{y}_i$. The summed square of residuals is given by:

$$SSE = \sum_{i=1}^{n} r_i^2 = \sum_{i=1}^{n} (y_i - \hat{y}_i)^2 \tag{5.1.1}$$

Where n is the number of datapoints included in the fit. The closer the SSE is to zero, the better is the fit estimate.
However, the to be fitted data must have a constant variance, meaning there must be no local disruptions. Within the restults there is the chance of quite some noise or other data. Therefore a weigthed least squared regression is made. An additional weight factor is included in the fitting proces minimising the error estimate:

$$SSE = \sum_{i=1}^{n} \omega_i (y_i - \hat{y}_i)^2 \tag{5.1.2}$$

Where ω_i are the weights which determine how much each datapoint influences the fitparameters.

5.1.2 R-Square

The R-square method measures how successful the fit is in explaining the variation of the data and is defined as the ratio of one minus the Sum of Square Error devided by the total Sum of Squares (SST).

$$\text{R-square} = 1 - \frac{\sum_{i=1}^{n} \omega_i (y_i - \hat{y}_i)^2}{\sum_{i=1}^{n} \omega_i (y_i - \bar{y})^2} \tag{5.1.3}$$

Where $\hat{y}_i$ is the value of the fitted datapoint, y_i the value of the specified datapoint, $\bar{y}$ the mean value and ω_i the weighting factor. R-square can take on any value between 0 and 1, with a value close to 1 indicating a better fit [11].

5.2 Weighted Fitting Method

Because of the possible slight differences between one resonance peak and another within actual measurements, the transmission spectrum may not be precisely periodic, leaving cftool to have difficulties with the altering shape. The experiments will be done to achieve raw data where a narrow resonance peak is more important than a wide resonance peak. Fitting two consecutive resonances gives an estimation of the resonance wavelengths, the FSR, the FWHM, the coupling and the powerloss inside the ring. The toolbox cftool tries to minimise the SSE over the whole length of the raw data therefore focussing on every datapoint as if it where equally important, adding a degree of difficulty to fitting the raw data. To counteract the last mentioned issue a weighting function is added.

$$\omega_i = \frac{1}{\sigma_i} \tag{5.2.1}$$

Here ω is the weight of the ith datapoint and σ the error of the corresponding datapoint. As can be seen, a larger error shows a smaller weight of the datapoint. This can be used for the space in between the resonance. It could be possible to have more than the desired amount of rings in the measured transmission spectrum. This can be visible in the space between the dips, concluding that these datapoints have the least importance and therefore the smallest weight. Giving all datapoints inside the dip a substancially larger weight than the datapoints in-between the dips helps cftool determine its best fit.

5.3 Fitting Method of Nonlinear Least Squares

When using a nonlinear function as fitting model, such as the periodic system transfer function, the nonlinear least squares formulation is used[12]. This method specifies an initial estimate for each coefficient, adjusts the coefficient and determines whether the fit improves. By default the toolbox uses the Trust-region algorithm to specify the direction and the magnitude of the adjustment of coefficient value. This is the only algorithm that can be used within cftool when contraints are added to the coefficient values.

5.4 Robust Nonlinear Least Squares

When one encounters a transmission spectrum with an exitential amount of noise (datapoints with local extreme values) it is possible to let cftool use the algorithm of Least Absolute Residuals (LAR). Datapoints that have a local extreme value, compared to the datapoints surrounding, have a large influence on the fit as squaring the error magnifies the effect. The LAR algorithm minimizes the absolute difference of the residuals; extreme values have less influence on the fit.

5.5 The complete fitting function

The system transfer function of the previous chapter was not yet complete as certain coefficients have to be added to facilitate MATLAB in finding the best fit of the model with the provided data of the results.
The first coefficient to be added is a coefficient that facilitates a horizontal shift of the entire fit, called fitparameter o. The second coefficient added facilitates a vertical shift of the entire fit, called fitparameter C. This fitparameter incorporates all losses due to non-critical coupling and the dark current. Dark current is the electric current flowing through an optical device when there are no photons entering the system.

Lastly there is one alteration made with the transfer function, instead of using the self coupling coefficient, the real part of the cross coupilng coefficient (κ) is used which translates to the self coupling coefficient in the following way:

$$c = \sqrt{1 - \kappa} \tag{5.5.1}$$

Where c and κ are both in normalised units between 0 and 1. With this alteration explained, the entire transferfunction used for the fitting of single ring resonance data is the following:

$$|H(\omega)| = |\frac{(\sqrt{1-\kappa}) - re^{-2\pi i(\omega+o)L}}{1 - (\sqrt{1-\kappa})re^{-2\pi i(\omega+o)L}}| + C \tag{5.5.2}$$

Where the following parameters are important:

- General coupling coefficient κ ranges from 0 to 1, unitless
- Round trip loss r ranges from 0 to 1, unitless
- Period L, in units of $[\lambda^{-1}]$
- Fitparameter o, in units of [nm]

- Loss fitparameter C, in units of normalised power

Of course this equation is only valid for the single all pass ring resonator. For the double all pass ring resonator changes have to be made to incorporate all double r, κ, L and o coefficients. The system transfer function will be dependent on the following coefficients:

$$|H(\omega)|_{double} = |H_1(\omega, r_1, \kappa_1, L_1, o_1)||H_2(\omega, r_2, \kappa_2, L_2, o_2)| + C \tag{5.5.3}$$

It could be said that if the single ring resonators designed the same, the coefficients of L_1 and L_2, o_1 and o_2 and r_1 and r_2 should be the same.
All measured results will be normalised to the insertionloss, therefore displaying a value between 0 and 1 that incorporates the insertionloss. Consequently the loss parameter C becomes in units of normalised power.

5.6 specifying fit options

By specifying certain fitting options the fitting procedure can be guided into the right direction for the purpose of saving time and aquiring physically acceptable values of coeficients. One of the fit options selected, the LAR algorithm, is already explained. Constraints were added to fitting parameters r and κ, as is explained another section. The maximum number of fit iterations allowed is set to 4000, where the default value is 400. The maximum number of model evaluations allowed is set to 6000, where the default value is 600. The termination tolerance used for stopping contitions is kept at the default value of 10^{-6}.

5.7 Fitcoefficient deviation error

The Curve Fitting Toolbox calculates confidence bounds for fitted coefficients. The confidence bounds define the lower and upper bounds of an interval. The estimated value of the fitting parameter lies inbetween this bounds, making the upper and lower bound an error margin of the fitting parameters value. These bounds are specified with a 95% certainty, meaning there is a 5% chance that the estimated value of the fitting parameter might lie outside of the confidence bounds.

Chapter 6

Experimental Setup

In the folowing chapter several experimental setups will be explained. The main subject of all setups is the Satrax box which is composed of a waveguide chip made by Lionix, a cooling mechanism and a controller interface connected to a computer of choosing. The layout of the chip is displayed in the figure below:

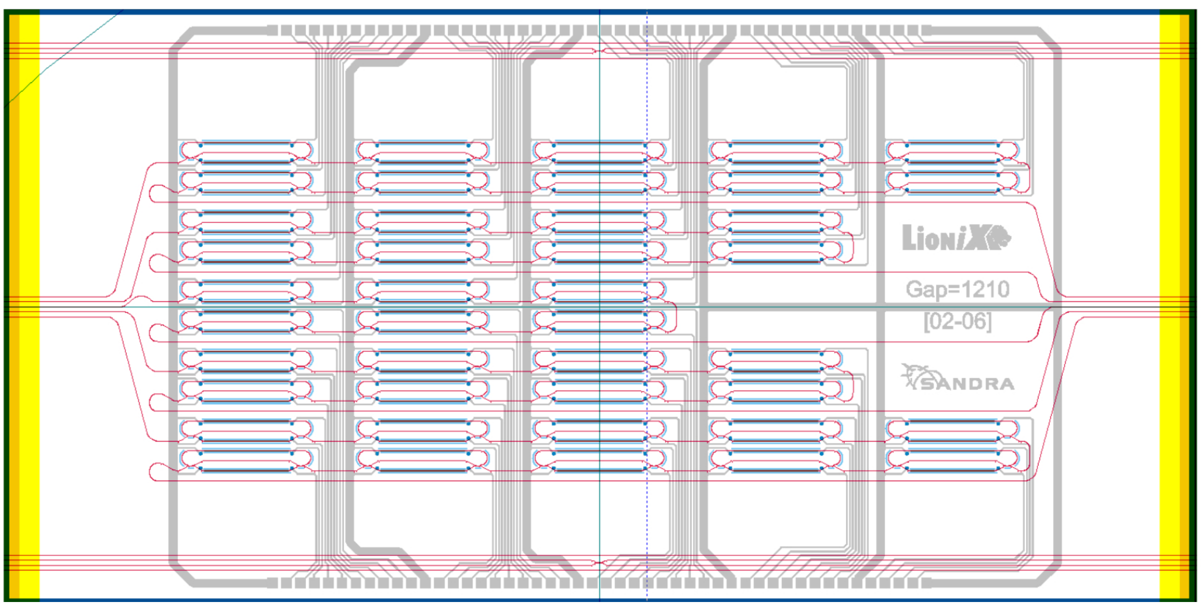

Figure 6.1: Layout of the Satrax box internal chip, image provided by Satrax.

The chip clearly shows five different tracks of rings, sets of six to ten sequential rings placed in series. In all of the experiments done, only one track of the chip was used, the third track with six sequential rings. For a more clear view, the following figure shows an zoomed in exerpt of the Satrax box chip:

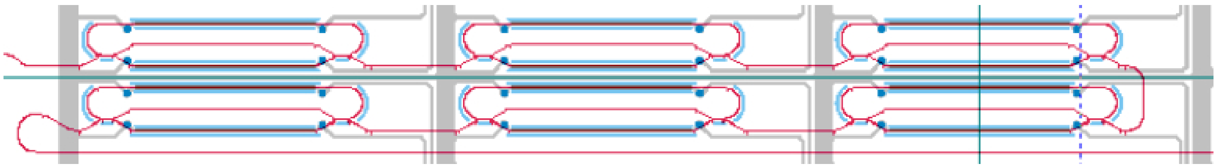

Figure 6.2: Zoomed in image of the third track of the Satrax box.

According to Satrax the following specifications are applicable to the chip:

- The chip is designed to have a ring circumference (geometrical length) of 6966.944 μm
- The coupling region is designed to have a gap width of 64.9 μm

To measure the transmission graph of the third track on the chip, a source and a reciever are necessary. A Superluminescent Diode (SLD) and an Optical Spectrum Analyser (OSA) were used as source and receiver respectively. The Satrax box was controlled by an external computer which also recorded the signal measured with the OSA. The setup can be viewed below:

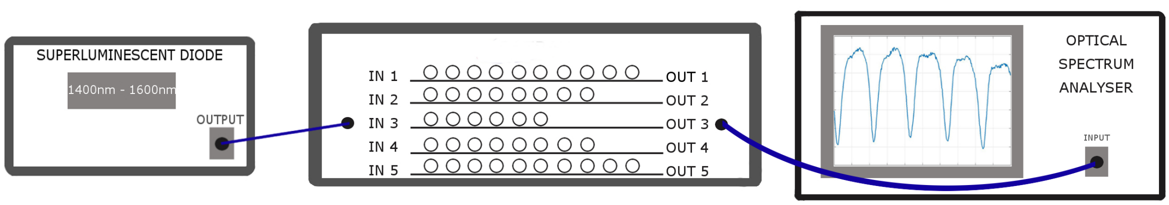

Figure 6.3: The total setup used for measuring the transmission graph of rings on the third track of the Satrax box chip. Please note that the image on the OSA is merely for esthetical purposes, it may not resemble a measured result.

The SLD used is from manufacturer Thorlabs with model number S5FC1005P and gives a wide distribution of power over a wavlength domain. There were two types of OSA used, both from manufacturer Ando with model number AQ6915 and AQ6917. The models distinguish themselfs in appliciations which were not used for these experiments and will therefore not be mentioned.

On the third track of the Satrax box, there are five kinds of measurements performed. The first measurement will be about loss inside the straight waveguide. The second and third measurement were performed on the third and fifth ring of the third track. The last set of measurements performed was the sequential coupling of the third and fifth ring. The two measurements done are different in the matching of resonance wavelength. The following setups indicate, in schematic overview, which rings were used.

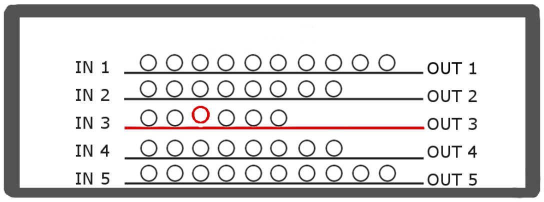

(a) Schematic overview of the third ring on the third track of the Satrax box

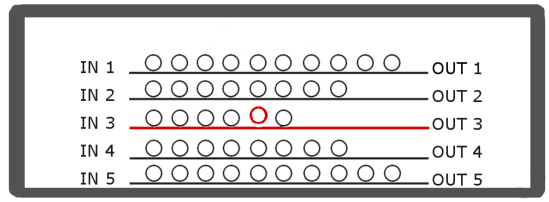

(b) Schematic overview of the fifth ring on the third track of the Satrax box

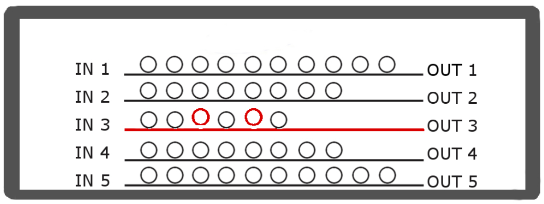

(c) Schematic overview of the third and fifth ring on the third track of the Satrax box

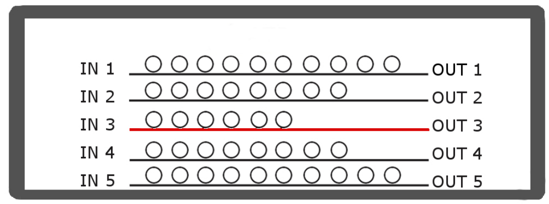

(d) Schematic overview of the straight third track waveguide of the Satrax box

Figure 6.4: Overview of used ring resonator configurations

To measure the reference value of the insertionloss, i.e. the direct signal of the SLD, the following setup was used.

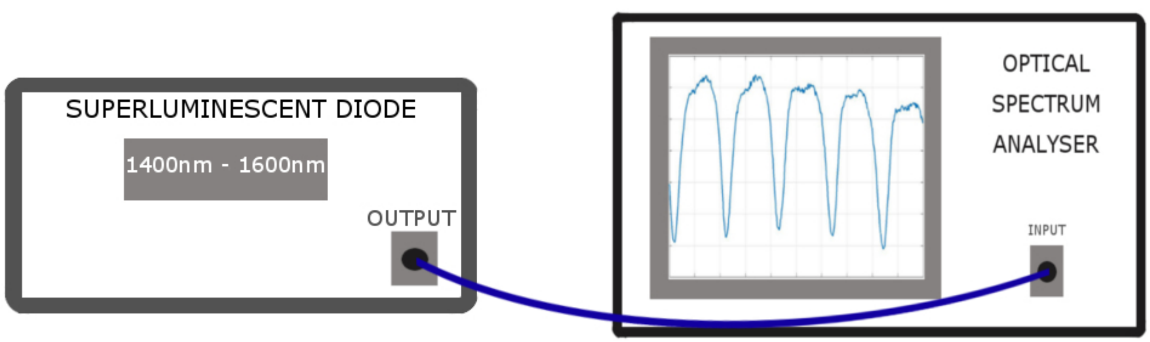

Figure 6.5: The total setup used for measuring the insertionloss reference value directly form the SLD. Please note that the image on the OSA is merely for esthetical purposes, it may not resemble the measured result.

The results of the measurements explained above will be explained in the next chapter.

Chapter 7

Results

In the following chapter, results measured with the setups from the experimental chapter will be shown and evaluated. The experimental data of each ring resonator will be fitted with the fitting model described in the corresponding chapter. From the final fit, the coefficients will be calculated and a comparison will be made to the geometrical length of the chip that Satrax provided. With the double ring results there is an added level of complexity, as the goal is to extract the information of two individual rings from one transmission graph.

7.1 Insertionloss

In the following section the powerlosses of the straight waveguide through the satrax box were measured. This amount of powerloss and the shape of the transmission graph through the satrax box are then used as a normalisation value for further measurments. The results in the figure below were substracted to eachother to get the insertionloss.

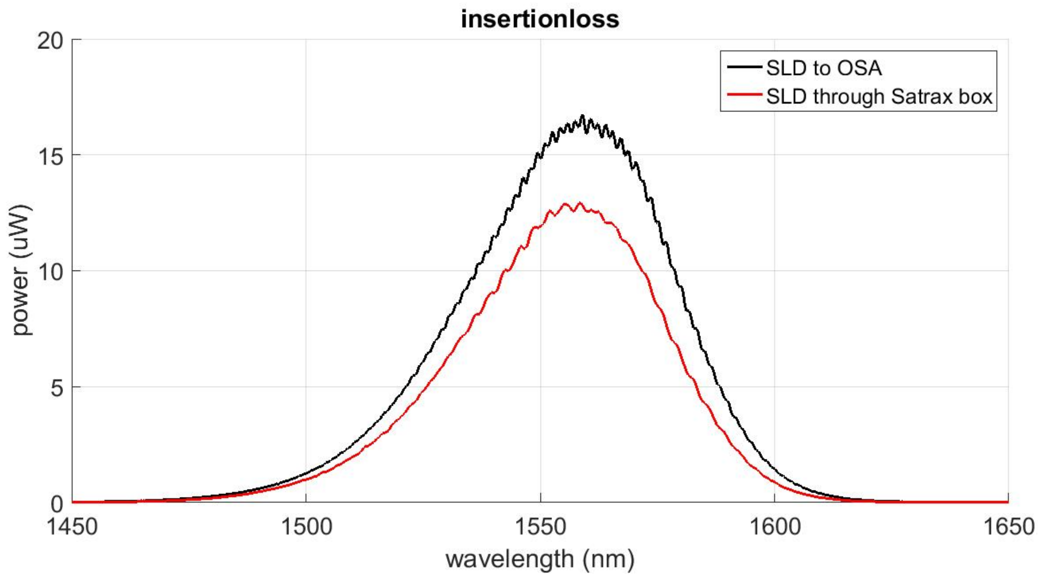

Figure 7.1: The transmission graph of the SLD, in black, versus the transmission graph of the Satrax box, in red. The difference in the maxima is 3.79 uW.

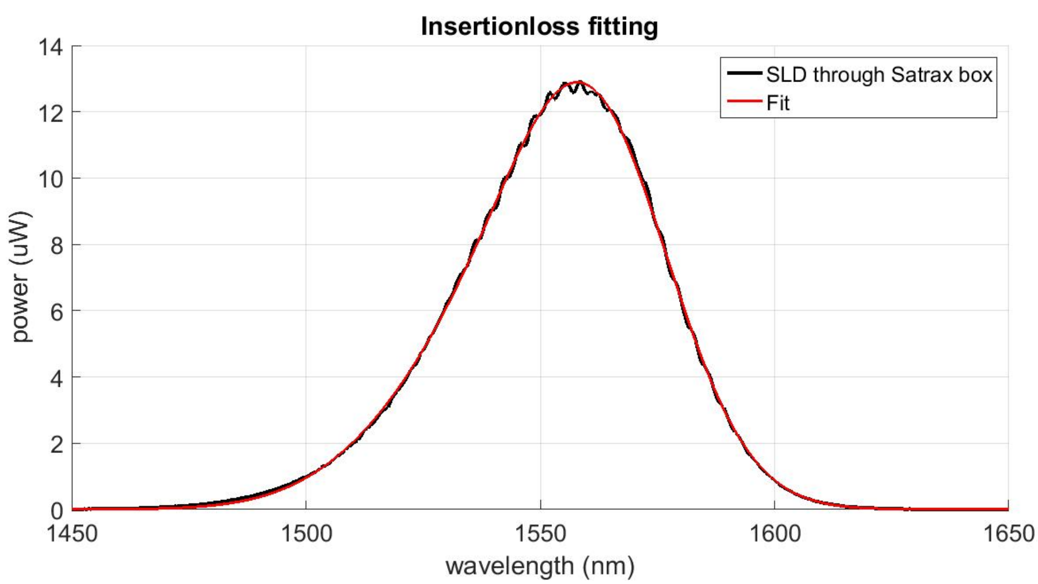

Figure 7.2: The fitted Gaussian of 2 terms over the raw data. SSE = 6.279 and $R^2 = 0.9997$.

Figure 7.1 clearly shows a difference in power between the source with and without the straight waveguide. When substracting the maxima of either graph the powerloss is 3.79 μW which can be translated into an overall powerloss of about 22.7%. hTis value of the insertionloss is dependent on the material properties of the waveguide inside the Satrax box i.e. internal reflections, index of refraction and the resistivity of the material.

To extract the normalisation values of the red line in figure 7.1, a fitting procedure has to be made. The amount of samples in figure 7.1 is 2001 over a domain of 200 nm. This represents a problem as the results of the single and double ring resonator have an amount of 1001 samples on the domain of 1 nm. There are simply not enough samples to do a pointwise normalisation. Therefore the figure of the insertionloss is fitted with a Gaussian. The fitting function is a superposition of two gaussians, due to the slight asymmetric shape of the graph. The fit of figure 7.2 becomes apparent.

This function of the fitted insertionloss can at any time be called by MATLAB to give the amount of necessary samples on the required domain therefore normalising the results presented in the next sections.

7.2 Single Ring Resonator

The third single ring was measured with setup 6.4a and resulted in the following transmission spectrum:

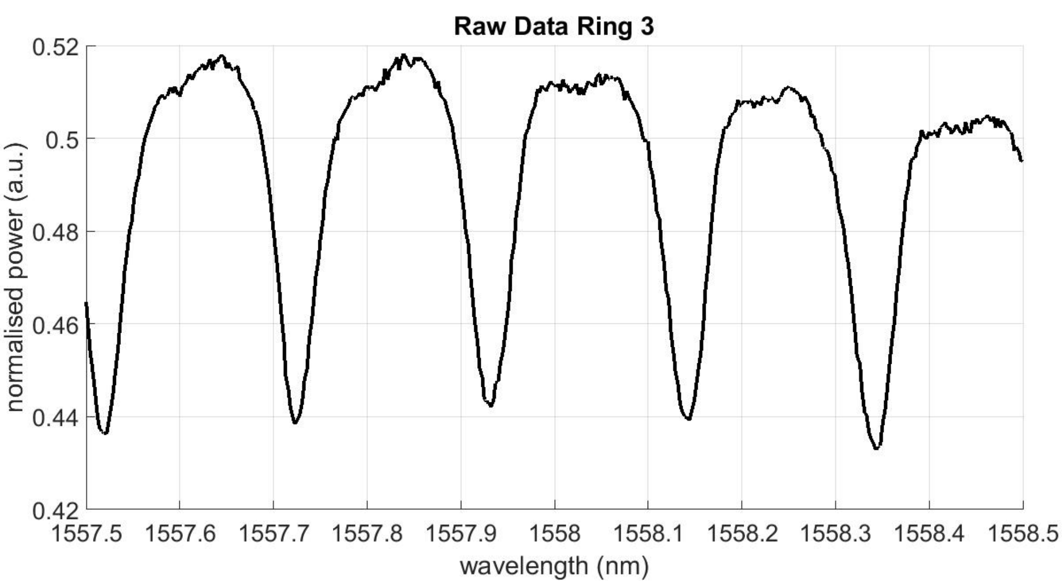

Figure 7.3: The transmission graph of the third ring on the third track of the Satrax box.

From this figure, a few statements can be made: The amount of peaks, the downward trend and the nonsymetrical shape of the peaks.

There are four peaks completely within the 1 nm domain of the wavelength and the peaks have a value of about 0.9 μW. The downward trend of the signal can either be due to the lightsource used (SLD), be due to an error of measuring or be due to a drift in the signal. The observation of the downward trend will be discussed in the fitting section. Apart from the downward trend some irregularities are observed in the space inbetween the resonance peaks. These top parts show a slight periodicity which could mean that, apart from the third ring, a second tranmission spectrum of another ring is still within the total signal. This would furthermore account for the fact that not all peaks are symmetrical.

The latter observation of the non symmetry in the figure has to be taken into account for the fitting procedure. A weighting fuction is added to force the fitting tool into viewing the non symetrical aspect of the figure as less important than the dips.

7.2.1 Fitting the raw data of ring 3

Before fitting the results as presented above, the normalisation has to be done. The reference value for the normalision is the fit of figure 7.2. The powerloss coefficient calculated is more likely to hold only the powerloss of the ring and not the powerloss of the straight waveguide.

If the downward trend is caused by the Gaussian shape of the SLD, it should be possible to incorporate the Gaussian shape into the fitting function which was done in the following way:

$$|H_{fitting}| = [\text{Gaussian Shape}]|[\text{System Transfer Function}] + C \tag{7.2.1}$$

Where the Gaussian shape of the source, as displayed in figure 7.2, is fitted by a superposition of two gaussian functions. As can be seen from the image below, the downward trend is fitted by the function proving that the downward trend is due to the transmission shape of the source. This same reasoning can be used for every other result that is presented in this chapter. The best fit of the model to the data is the displayed in figure 7.4.

From the SSE and the R^2 can be seen that the fit is quite decent as the R^2 is close to one. When looking at the normalised power axis it can be seen that there is not a 100% transmission of the ring resonator, this difference will further show itself in the fitparameter C and the coefficient r. The fitting parameters and coefficients taken from the model are:

κ	0.08152 $\pm$ 0.002
r	0.4021 $\pm$ 0.012
L	4.8705 $\pm$ 0.002
o	-38.35 nm $\pm$ 0.35 nm
C	-0.5246 $\pm$ 0.001

From coefficient κ, the self coupling coefficient can be calculated, which results in: c = 0.9583 $\pm$ 0.006.

When using boundaries on one or several coefficients, starting conditions of the coupling coefficient and the powerloss coefficient must be given. It is assumed that the ring

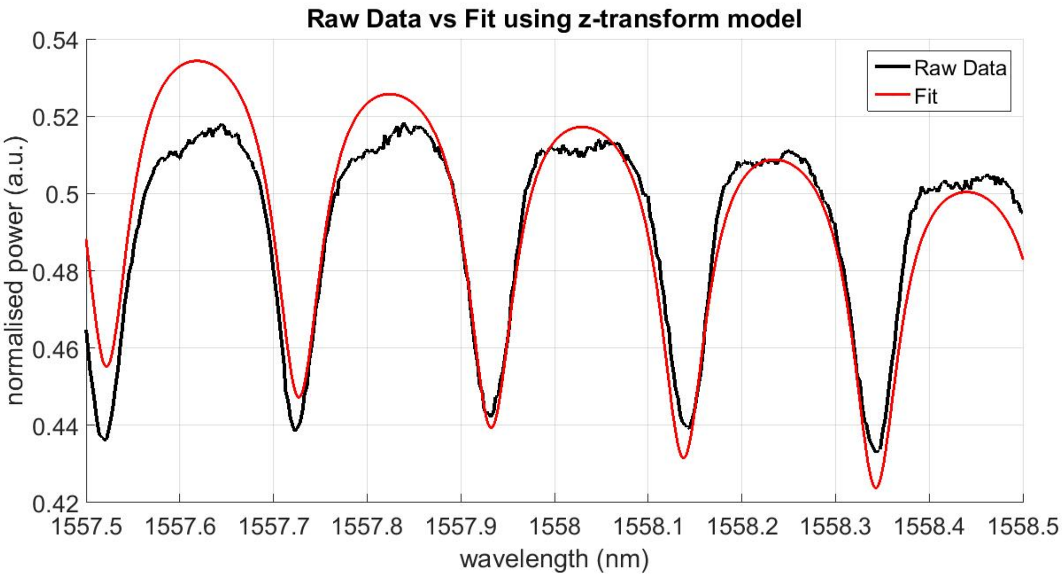

Figure 7.4: The calculated fit over the transmission graph of the third ring on the third track of the Satrax box with SSE = 0.9346 and R^2 = 0.9989.

is in critical coupling which means that the value of κ should be the same as the value of r. That is why the coefficients κ and r have startingconditions taken to be 0.5 In every round trip about 95% of the light inside the ring will stay within the ring leading to stronger interactions between the light from multiple roundtrips in the ring. The powerloss coefficient r shows that after one roundtrip, 48% power is still within the ring. This is an understandible limit and a reasonable value accounting the fact that the rings of the Satrax box are quite large, i.e. larger than 1 mm in radius [13][14][15] according to the manufacturers details. The coupling coefficient does not have nearly the same value as the powerloss coefficients, which means the ring is overcoupled to the straight waveguide. An observation that can also be done when looking at the lowest value of the dips because when in critical coupling the lowest value should be zero percent.

There is no physical purpose to fitting parameter o, therefore it will not be discussed. The fitting parameter L, will be translated to the FSR in the next section. The last fitting parameter to be discussed is the offset parameter C, which accounts for further losses of the system. As the system is not in critical coupling, there is a powerloss in the coupling region, displayed by fitting parameter C.

7.2.2 Characterisation of ring 3

The parameters from the fit can be used for further caracterisation of the measured ring resonator, as explained in the theoretical chapter. The following values for several characteristics were calculated:

FSR	0.2052 nm ± 0.0005 nm
FWHM	0.0537 nm ± 0.001 nm
Finesse	3.8220 ± 0.5
$L_{optical}$	11821 μm ± 16 μm
$L_{geometrical}$	6896.9 μm ± 9.3 μm
Radius	1097.7 μm ± 1.5 μm

The calculated numbers show the caracteristics of the measured ring, which can be related back to the original data that the manufacturer provided by the system. A ring with a Finesse of about 4.3 ± 0.5 is a low finesse ring, which means that the measured ring resonator device is sensitive to a wide range of resonances. A higher finesse device, at least an order of 10 higher, has a less wide range of resonances and is less accurate in displaying the rings resonance wavelengths [16]. The calculated optical length, geometrical length and the radius of the measured ring are actually quite close to the manufacturers data. As said before, the geometrical length of the ring was designed to be 6966.944 μm long where the calculated length is 6872.2 μm ± 9.4 μm. Even within the error margin, these values differ. This could be due to a fabrication error of the waveguide chip, but it could likewise mean that there is a measuring error within the raw data.

In the next section the fifth ring of the third track will be presented and evaluated. Much of the same resoning will be applied, there will be a less comprehensive explanation of certain observations. At the end of the evaluation of the fifth ring there will be a discussion on the similarity between the measurments of ring three and ring five.

7.2.3 Third track, fifth ring

With setup 6.4b the following tranmission spectrum of a single ring resonator was measured: In the figure above, there are five dips clearly visible within the 1 nm domain of the wavelength and the peaks have a value of about 0.9 μW. With this spectrum the downward trend due to the source of the light is even more apparent than with ring number three. There are some irregularities in the space inbetween the resonance dips which show no apparent periodicity. Therefore the irregularities can be noise and are assumed to not be another ring resonator being coupled in apart from ring number five. With the fitting of this tranmission graph, a weighting function is used to give less notice to the noise.

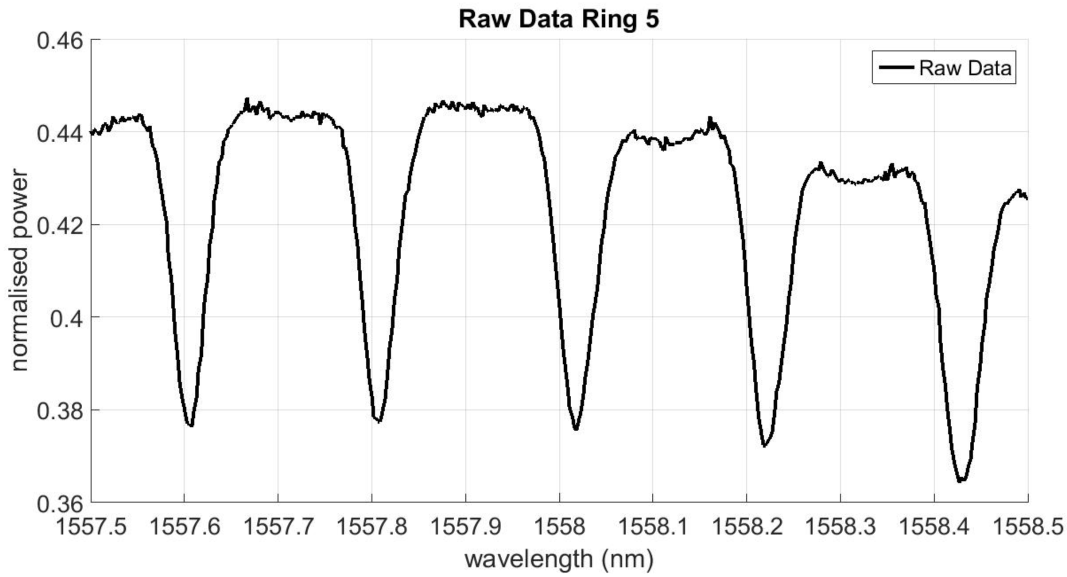

Figure 7.5: The transmission graph of the fifth ring on the third track of the Satrax box.

7.2.4 Fitting the raw data of ring 5

The normalisation was done in the same manner as with the results presented in the previous section. The Gaussian shape of the source was added to the model in the same way as in the previous ring.

The best fit of the model to the data is the following one:

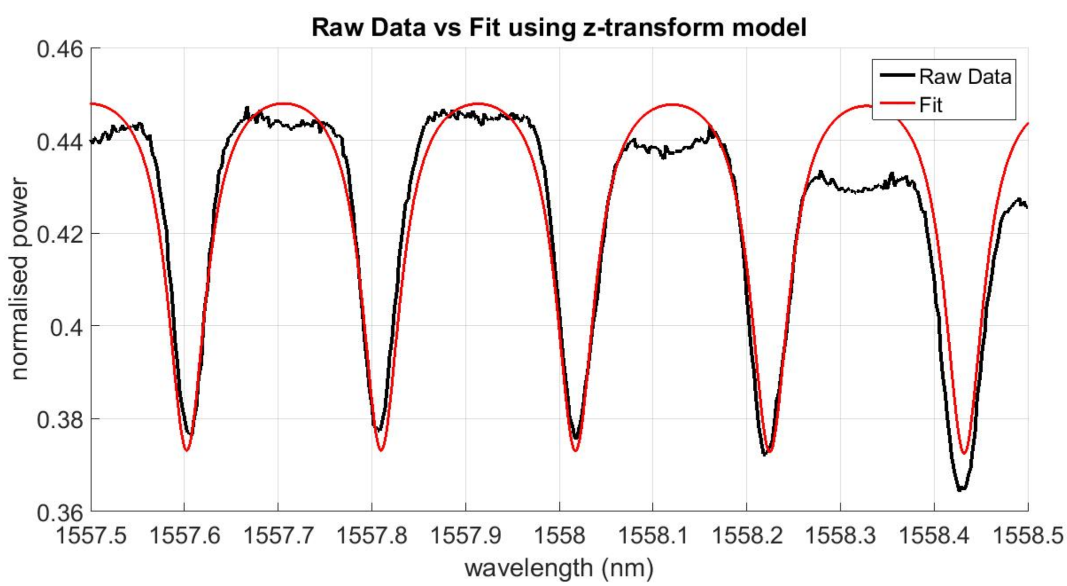

Figure 7.6: The calculated fit over the transmission graph of the fifth ring on the third track of the Satrax box with SSE = 0.6517 and R^2 = 0.9975

From the SSE and the R^2 can be seen that the fit is decent as R^2 is again fairly close to its maximum value, 1. When looking at the normalised power axis it can be seen that there is no 100% transmission of the ring resonator, this difference will further show itself in the fitparameter C and the coefficient r. The fitting parameters and coefficients taken from the model are:

κ	0.0627 $\pm$ 0.006
r	0.4727 $\pm$ 0.006
L	4.8215 $\pm$ 0.001
o	-22.44 nm $\pm$ 0.24 nm
C	-0.5377 $\pm$ 0.0015

From coefficient κ, the self coupling coefficient can be calculated,: $c = 0.9681 \pm 0.006$. Starting conditions of 0.5 were given for r and κ as it was assumed that the rings were in critical coupling. In every round trip about 99% of the light inside the ring, stay's within the ring. The round trip powercoefficient of 48% is slightly larger than the powerloss coefficient of the third ring, but it is within understandible limits. The coupling coefficient does not have the same value as the powerloss coefficient, meaning the ring is overcoupled to the straight waveguide.

The fitting parameter L, can be translated to the FSR, explained in the next section.

7.2.5 Characterisation of ring 5

The parameters from the fit can be used for further caracterisation of the measured ring resonator, as explained in the theoretical chapters. The following values for several characteristics were calculated:

FSR	0.2074 nm $\pm$ 0.0005
FWHM	0.0462 nm $\pm$ 0.001
Finesse	4.4902 $\pm$ 0.5
$L_{optical}$	11704 μm $\pm$ 16 μm
$L_{geometrical}$	6828.6 μm $\pm$ 9.3 μm
Radius	1086.8 μm $\pm$ 1.5 μm

The calculated numbers show the characteristics of the measured ring, which can be related back to the original data that the manufacturer provided. The fifth ring shows a Finesse of about 4.2 which is, much like the third ring, a low finesse value. The calculated optical length, geometrical length and the radius of the measured ring again deviate from the manufacturers data provided. As said before, the geometrical length of the ring was designed to be 6966.944 μm long where the calculated length is 6846.7 μm $\pm$ 9.3 μm.

7.2.6 comparison of ring 3 and ring 5

A few comparisons between both single ring experiments were made in the text but they will revisited in this section. The coupling coefficients and the powerloss coefficients are within there error margins the same for both rings. One of the comparisons that can be discussed is the maximum value of the raw data transmission graph as the power with ring three is higher than with ring five. This could be explained by the presence of more than one coupled ring in the transmission spectrum with ring five, which would likewise mean that the influence of one extra ring was larger in the measurement of ring five compared to ring three. The next comparison can be made between the FSR, the FWHM and the Finesse. The deviation between the two Finesse values was not to be expected as the FWHM and the FSR of both rings are approximately the same. The last comparison is of the geometrical length, as both rings were designed with a geometrical length of 6966.944 μm and the values calculated with the fitted transmission graphs slightly deviate. But, when considering the amount of losses and the non-ideal tranmission graph measured, both values calculated for the geometrical length are satisfactory. The general conclusion can be made that indeed, ring three and ring five are of approximately the same radius and composition.

For the purpose of the double ring resonator fitting model all optical coefficients (k,r and L) of ring three and five are taken as initial values for the fitting procedure.

7.3 Double Ring Resonator

The double ring resonator is a very different system to evaluate than the single ring resonator, mainly because of its greater sensitivity to errors. There are further complications with the double transferfunction used to fit the raw data, as the double amount of fitting coefficients is more complex. In the following section, two types of transmission graphs will be evaluated. One with the matching resonances and one with non matching resonances. From both transmission spectra the ring characteristics will be extracted.

7.3.1 Overlapping resonance wavelength

With the setup provided figure 6.4c the following tranmission spectrum of a double ring resonator was measured:

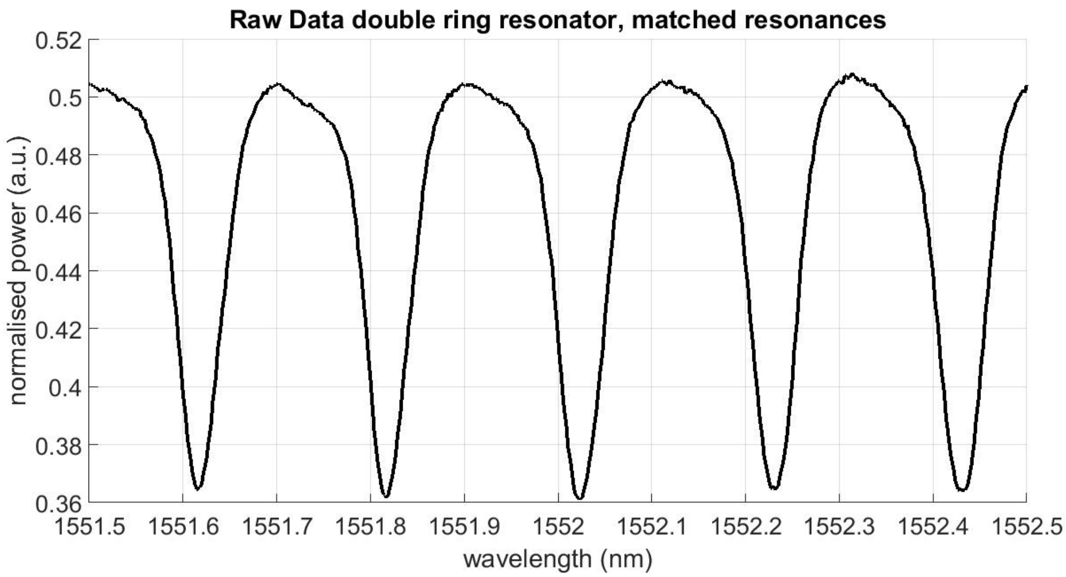

Figure 7.7: The transmission graph of the third and fifth ring on the third track of the Satrax box.

The double ring resonator has a large difference of power along the power axis compared to the single rings. There is about a 4 μW difference between the top and the bottom of the transmission figure. There is not an apparent downward trend but instead a slight upward trend. The wavelength domain of the measurement is different from the measurements before, as the domain reaches from 1551.5 nm to 1552.5 nm. The shape of the source seems to have a lesser influence on this domain than with the previous domains. The former observation can be proven by fitting the data. The parts inbetween the dips are not smooth, even when one looks past the obvious noise there is still a slight extra dip visible, which suggest there are more than two rings inside this tranmission spectrum.

Again a weighting fuction is added to force the fitting tool into viewing the slight non symetrical aspect of the figure as less important than the dips.

7.3.2 Fitting the raw data of the double ring resonator

The normalisation of the raw data was done a bit different from the single ring resonators. As the double ring resonator has the double amount of losses due to the straight waveguide, the reference normalisation value is doubled. The slight upward trend is fitted by the model function proving that the trend is due to the transmission shape of the source. The best fit of the model to the data is the following one:

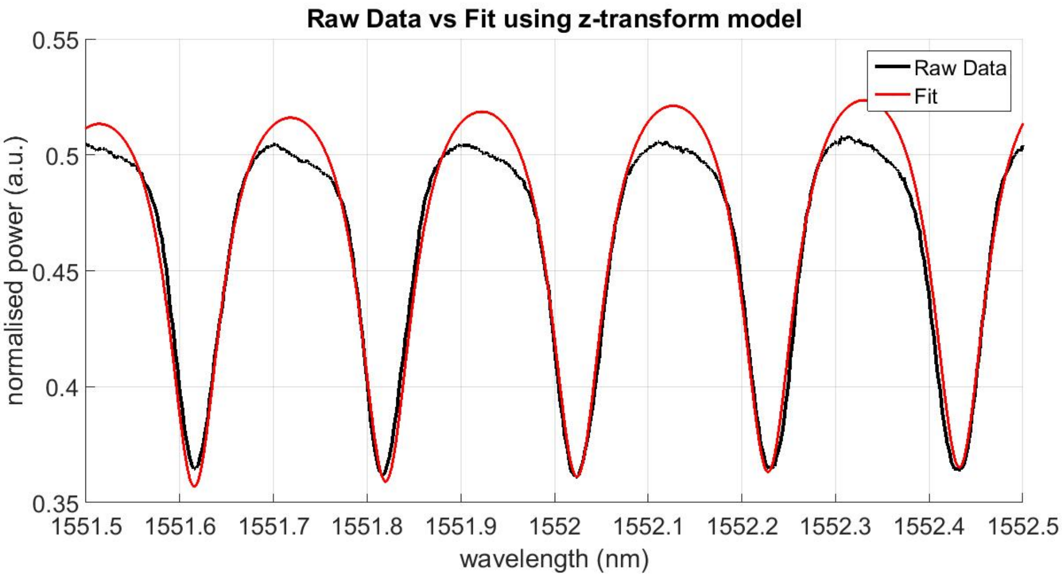

Figure 7.8: The calculated fit over the transmission graph of the double ring experiment on the third track of the Satrax box with SSE = 1.276 and R^2 = 0.9988.

From the SSE and the R^2 can be seen that this is a decent fit as both numbers are within reasonable range to their ideal values. The fitting parameters and coefficients taken from the model are:

κ_1	0.10960 ± 0.0036
κ_2	0.10999 ± 0.0032
r_1	0.35942 ± 0.008
r_2	0.35931 ± 0.009
L	4.89770 ± 0.005
o	-84.61834 nm ± 0.24 nm
C	-0.38755 ± 0.013

As one assumes that the resonances of the rings are matched by tuning them such in the measuring process, the fitting parameters L_1 and L_2 are reduced to L. From coefficients κ_1 and κ_2, the self coupling coefficients can be calculated: $c_1 = 0.9436 \pm 0.006$ and $c_2 = 0.9436 \pm 0.006$.
It is not possible to state wich set of coefficients account for which ring with matched resonance wavelengths. Therefore the single rings will not be called by their position on the straight waveguide, but simply by A and B. A different way of working was used for determining the starting conditions of the fit. Instead of using the critical coupling conditions, the parameter values of previous experiments were used as a starting condition.

The fit shows that it is possible to extract single ring resonator coefficients from a double ring resonator but the question arises of the accuracy of the values compared to the extracted values of the single ring experiments.

It is possible to remodel the single rings of the double ring experiment by filling in the fit-paramaters into the fitting function. The resulting graphs over the raw data are visualised in the figure below:

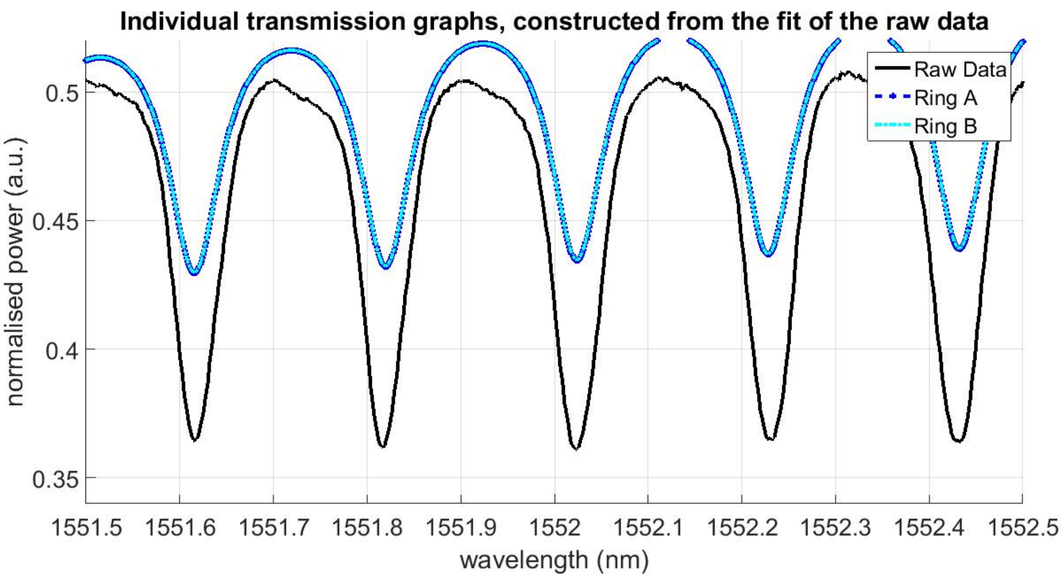

Figure 7.9: The reconstructed fit over the transmission graph of the double ring experiment on the third track of the Satrax box.

Although the values of the fittingparameters for ring three and ring five might differ slightly, their transmission spectra are identical to eachother. Therefore that the double ring setup was made up out of two rings with the same radius and internal composition. The whole system is still in overcoupling as the roundtriploss is larger than the amount of light that couples in to the looped waveguide for both rings.

7.3.3 Characterising the Double Ring Resonator

By remodeling the single ring resonators of the double ring experiment, the characterisation can be done on the single rings instead of a double system, providing more accuracy on the individual rings. The FSR, FWHM and Finesse can be calculated for a specific ring, instead of the whole filter. The optical length, geometrical length and the radius can likewise be calculated with higher accuracy for the single rings. The following values for several characteristics were calculated:

FSR	0.2042 nm ± 0.0005 nm
$FWHM_{ringA}$	0.0598 nm ± 0.001 nm
$FWHM_{ringB}$	0.0598 nm ± 0.001 nm
$Finesse_{ringA}$	3.4129 ± 0.5
$Finesse_{ringB}$	3.4250 ± 0.5
$L_{optical}$	11791.4 $\mu m \pm 20$ μm
$L_{geometrical}$	6879.5 $\mu m \pm 11.6$ μm
Radius_2	1094.9 $\mu m \pm 1.8$ μm

As the parameter L was taken because of matched resonances, there is only one value for the FSR which can be applied to both single rings. Because the transmission spectra of ring five and three are of matched resonances and of identical FSR due to only one L fitting parameter, the optical length, geometrical length and radius of both rings are the same.

The calculated numbers show the caracteristics of the measured two ring system, which can be related back to the data of the manufacturer and the single ring experiment. The Finesse of the rings are not identical, which suggest that the transmission spectra of both rings are not completely identical. The digits that account for the difference are at least in the order of magnitude one over tenthousand. Still these small variations seem to make a sligtly larger difference in the characterisation values. The geometrical length of the rings was designed to be 6966.944 μm long where the calculated length is 6879.5 $\mu m \pm$ 11.6 μm. The designed length is 87.4 μm longer than the measured value.

7.3.4 Distinquisthable resonance wavelength

In this section the tranmission graph of the double ring experiment is presented where the resonances of either ring are not matched. With the setup provided in figure 6.4c the tranmission spectrum of figure 7.10 was measured. It can be seen from figure 7.10 the length of the peak along the power axis is smaller than with figure 7.7. There is about a 1.2 μW difference between the top and the bottom of the dip and similar to the previous results of the single ring resonator there is a slight upward trend visible. The domain of the measurement is the same as the previous double ring result.
Different from the results mentioned before, the parts inbetween the dips are quite smooth.

7.3.5 Fitting the raw data of the double ring resonator

The best fit of figure 7.10 is presented in figure 7.11. As can be seen from figure 7.11, the slight upward trend is fitted the fitting function proving that the trend is due to the transmission shape of the source. To be able to fit the separated peak a separation of fitparameter o to o_1 and o_2 was done to accomodate two horizontal shifts.

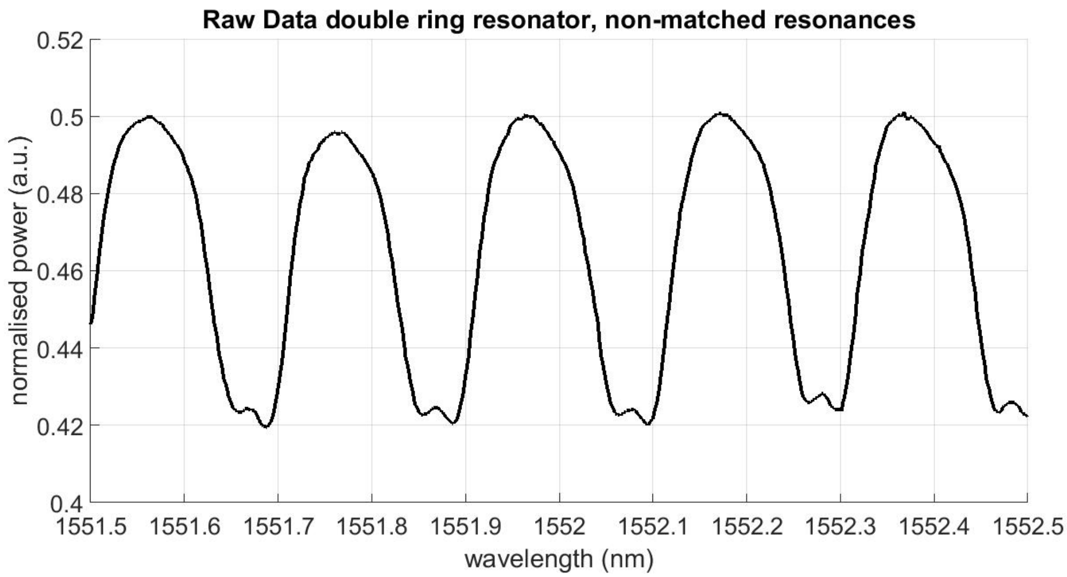

Figure 7.10: The transmission graph of the third and fifth ring on the third track of the Satrax box with the resonance wavelength of each ring visibly apart. The left peak corresponds to the fifth ring, the right peak corresponds to the third ring.

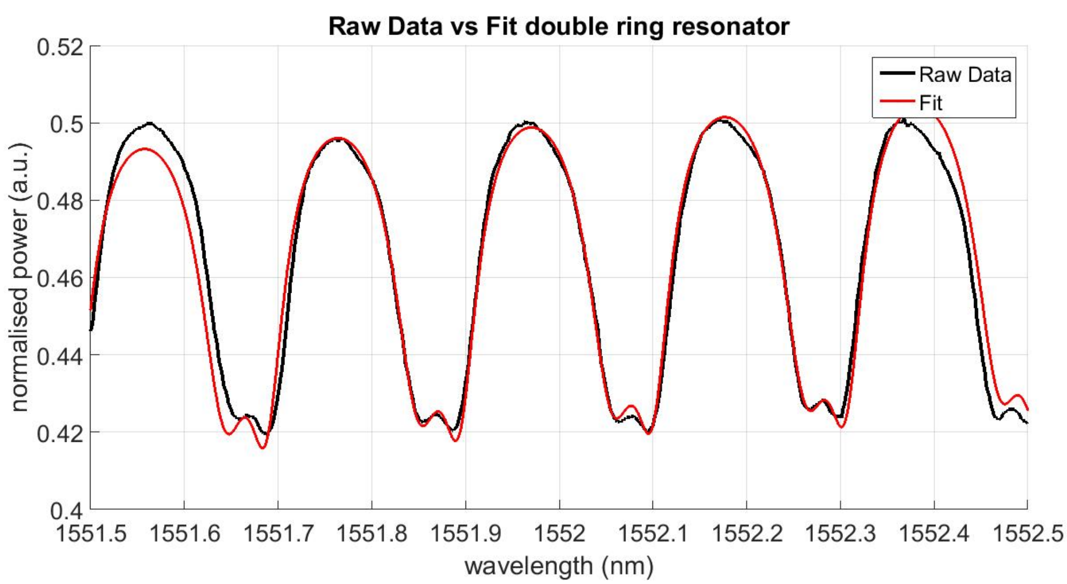

Figure 7.11: The calculated fit over the transmission graph of the third ring on the third track of the Satrax box with SSE = 0.004279 and $R^2 = 0.9952$.

From the SSE and the R^2 can be seen that this is a decent fit as both values are close to their ideal value. The fitting procedure was able to fit the double peak at the bottom of the transmission line but suggests a slightly larger steady increase of power over the wavelength domain. The fitting parameters and coefficients taken from the model are:

κ_1	0.05451 ± 0.002
κ_2	0.08359 ± 0.003
r_1	0.4886 ± 0.017
r_2	0.3699 ± 0.015
L_1	4.8530 ± 0.005
L_2	4.8280 ± 0.005
o_1	-73.07 nm ± 0.33 nm
o_2	-83.58 nm ± 0.17 nm
C	-0.4285 ± 0.002

All coefficients with subset number 1 correspond to ring number five, consequently all coefficients with subset number 2 correspond to ring number three. From coefficients κ_1 and κ_2, the self coupling coefficients can be calculated: $c_1 = 0.9724 \pm 0.006$ and $c_2 = 0.9573 \pm 0.006$. The starting conditions used for the double coefficients are the same as with the double experiment done before.

Much like the first set of double ring resonator results, this fitting procedure has shown that the slight upward trend was due to the shape of the source, as the model is able to fit the trend with the signal.

From the fitparameters is it clearly visible that it is possible to extract the single ring coefficients from the double ring tranmission spectrum. It is comforting to see that the values of r and κ of ring three resemble the corresponding coefficientsvalues of ring five. A observation has to be made in the difference of L_1 and L_2 as they differ an order of magnitude larger than the appointed error region. If the single rings are of the same composition, the different L should not be the case. Furthermore it seems that ring number five is more inclined to critical coupling behaviour than ring number three.

It is again possible to remodel the single rings of the double ring experiment by filling in the fitparamaters into the fitting function. The resulting graphs over the raw data are visualised in figure 7.12.

The graph clearly shows the two different rings, with ring three slightly less coupled than ring number 5. Therefore that the double ring setup was made up out of two rings with the same radius and internal composition. The whole system is still in overcoupling as the roundtriploss is larger than the amount of light that couples in to the looped waveguide for both rings.

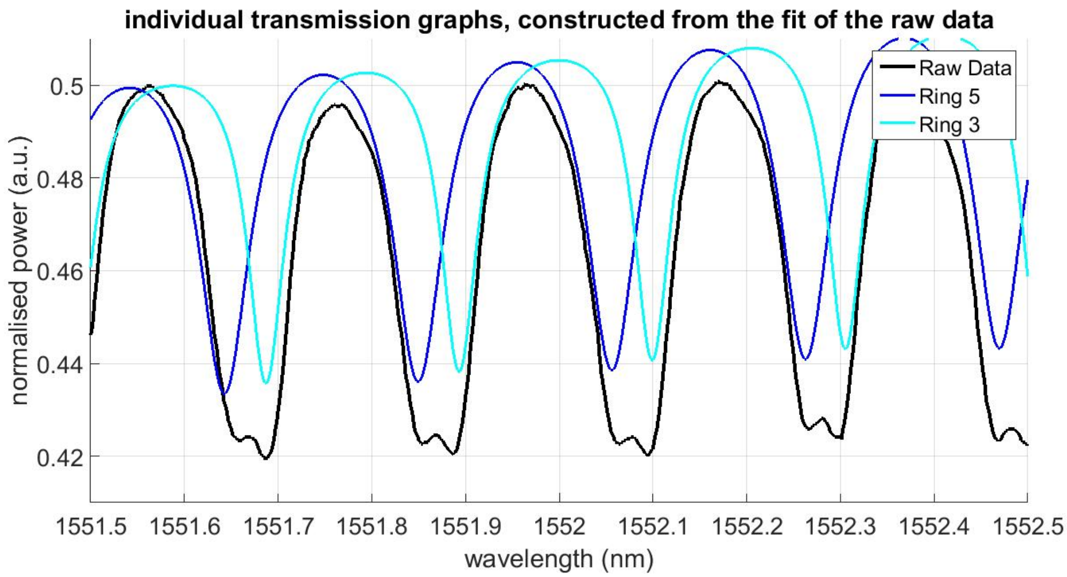

Figure 7.12: The reconstructed fit over the transmission graph of the double ring experiment on the third track of the Satrax box.

7.3.6 Characterising the Double Ring Resonator

The measurements were done with the same setup as with the previous double ring experiment, therefore the optical length, geometrical length and radius must be the same compared to the previous experiment. The following values for several characteristics were calculated:

FSR_1	0.2061 nm $\pm$ 0.0005 nm
FSR_2	0.2067 nm $\pm$ 0.0005 nm
$FHWM_1$	0.0595 nm $\pm$ 0.001 nm
$FWHM_2$	0.0457 nm $\pm$ 0.001 nm
Finesse$_1$	3.4748 $\pm$ 0.5
Finesse$_2$	4.5094 $\pm$ 0.5
$L_{optical1}$	11684.14 $\mu m \pm 20$ μm
$L_{optical2}$	11647.83 $\mu m \pm 20$ μm
$L_{geometrical1}$	6816.9 $\mu m \pm 11.6$ μm
$L_{geometrical2}$	6795.7 $\mu m \pm 11.6$ μm
Radius$_1$	1084.9 $\mu m \pm 1.8$ μm
Radius$_2$	1081.6 $\mu m \pm 1.8$ μm

The first observation to be made is the inequality of both FWHM's as they differ quite an amount from eachother. This can likewise be observed from the reconstructed single ring models and in the coefficients r and κ corresponding to the rings. Though ring number three has a higher cross coupling and a lower round trip loss, the values of these coefficients are closer to eachother meaning a better coupling of the ring compared to ring number five. Likewise can be stated that better coupling accounts for a more narrow peak, resulting in a higher finesse. The optical length, geometrical length and radius of the individual rings are approximately of the same value, though stretched within their error regions. Again the digits in parameters L_1 and L_2 that account for the slight difference in $L_{optical}$, $L_{geometrical}$ and R are in the order of magnitude one over thousand. These small variations make a sligtly larger difference in the characterisation values. The geometrical length of the rings was designed to be 6966.944 μm long where the calculated length of the single rings, on average, 6806.3 μm ± 11.6 μm. The designed length is 160.644 μm longer than the measured value. The last mentioned difference of experimentally measured value with designed fabrication value is almost twice as large as the difference value corresponding to the previous double ring experiment. This could be due to the increased complexity of having a fitting function with almost double the amount of fitting parameters.

7.3.7 Fitting overlapping or distinguishable resonance wavelengths

The fitting model can be altered to have less or more fitting coefficients, depending on the transmission spectrum to be analysed. When the resonance wavelengths are matched there is no need for two different coefficients L and o. One could say that with less fitting coefficients the accuracy of fitting the transmission spectrum is less, but this does not seem the case. The fitting procedure does seem able enough to combine the coupling coefficient and the round trip powerloss until the two have a value to match the raw data. Due to the addition of parameters for the non matching resonator wavelengths the fitting procedure is more vulnerable to error, therefore one could state this is less accurate than the matching resonator wavelengths.

When measuring the overlapping resonance wavelength one is not completely sure if there are two rings and if they are exactly on the same resonance wavelength but when that assumption is made, fitting the results is less complicated than with the results of figure 7.10.

Chapter 8

Conclusion

In the process of fabrication of a waveguide chip, there are certain errors of manufacture that have to be taken into account. Only the designed dimensions of a waveguide network are known when receiving the fabricated chip, which could differ with the actual values. In fabrication the layer thickness can be controlled very accurately, up to ten atom thickness, therefore a one or two atom error is not of that much consequence. But in the lithograpy of the networks geometry there are errors possible of 50 μm which is comparable with the wavelengths send through the system. The fabrication of the gap is also a problem. A small gap between the looped waveguide and the straight waveguide leaves a large susceptibility to fabrication error. The scale upon which lithography can be performed is one micrometer, if an error of 0.5 μm is introduced, the width of the gap is changes significantly. As the evanescent field is stronger when closer to another waveguide even a small variation of the width can affect the coupling coefficients. The difference in designed value and actual value can have a large effect in the actual workings and applications of the waveguide network. It is therefore important that there is a way to question the designed values by measuring these optical and geometrical properties yourself.

By analysing transmission spectra of ring resonator networks with a known geometry certain characterising coefficients can be extracted: the coupling coefficients, loss coefficients and quality factors, such as Finesse and geometrical length of the looped waveguide networks.

Analysing the transmission spectra is done by a system transfer function in the z-domain, converted into a fitting model with parameters corresponding to the above mentioned characterisation coefficients.

A downward trend was visible in the output measured signal data, which is due to the overal signal shape of the lightsource used in measuring. The SuperLuminescent Diode showed a general shape, a-symmetric and comparable to a gaussian function, stretched over a domain of about 200 nm.

Four different transmission spectra were analysed: two single all pass ring resonators and

two times a double all pass ring resonator system, composed out of the two single rings previously mentioned. The first of the single ring resonators has a self coupling coefficient of 0.9583 ± 0.006, a round trip loss of 0.4021 ± 0.012 and the looped waveguide has a geometrical length of 6896.9 μm ± 9.3 μm. The second of the single ring resonators has a self coupling coefficient of 0.9681 ± 0.006, a round trip loss of 0.4727 ± 0.006 and the looped waveguide has a geometrical length of 6828.6 μm ± 9.3 μm. The designed length of the looped waveguide is 6966.944 μm, which is not near the designed value given by the manifacturer; the characteristic extracted by the measurement differs for about 100 μm. It can be concluded that the measured single rings must be indeed of the same composition as designed, because their value of geometrical length is closer to eachother than the designed length.
The double ring resonator is composed out of the previously mentioned single ring resonators, coupled in series. There are two measurements done with this configuration of rings, one with matched resonances and one with non matching resonances. With the first measurement one assumes the resonance wavelengths are completely matched by tuning them such in the measuring process. It is possible expand the fitting model to incorporate more than one ring and extract two sets of coefficients, one for each ring. However it is not possible to state which set of coefficients correspond to which ring. According to the double ring experiment the self coupling coefficients of the first and second ring are 0.10960 ± 0.0036 and 0.10999 ± 0.0032, their round trip losses 0.35942 ± 0.008 and 0.35931 ± 0.009 and the geometrical length calculated with matched resonances of 6879.5 μm ± 11.6 μm. The designed geometrical length is about 87.4 μm longer than the measured value.
The second double ring measurement was done with non matching resonance wavelength. To accomodate for the double peak transmission spectrum, a second set of variables had to be added to the fitting procedure, increasing the probability of errors whithin the fitting procedure. Because one has two peaks visible in the transmission spectrum which are tuned manually in the measuring process, one can state beforehand which set of variables will correspond to which ring. According to the second double ring experiment the self coupling coefficients of the first and second sequentially coupled rings are 0.08359 ± 0.003 and 0.05451 ± 0.002 respectively, their round trip losses 0.3699 ± 0.015 and 0.4886 ± 0.017 respectively and the geometrical length calculated 6795.7 μm ± 11.6 μm and 6816.9 μm ± 11.6 μm. The designed geometrical length is about 160.644 μm longer than the measured value, which is almost twice as large as the difference value corresponding to the previous double ring measurement. This could be due to the incresed complexity of having a fitting function with almost double the amount of fitting parameters. The self coupling coefficients of the non matching resonance double ring experiment are of the same order of magnetude as the corresponding single ring resonator experiments.
On a more general note one could state that less fitting parameters result in a lower accuracy of the fitting procedure. More fitting parameters can result in a higher accuracy of the fitting procedure but it can likewise result in higher error of coefficients. Due to the addition of parameters for the non matching resonator wavelength the fitting procedure is more vulnerble to error, therfore one could state this is less accurate than the matching resonator wavelengths provided that the resonator wavelengths are completely matched.
It is proven that resonator characteristics such as coupling coefficients, loss coefficients

and geometry characteristics can be extracted from diffent kinds of transmission spectra. Not only of transmission spectra with only a single ring resonator, but likewise with systems of double ring resonators.

Chapter 9

Recommendations

During this assignment, there were some problems with the setup and the fitting procedure.
The Satrax box consists out of a waveguide chip and a cooling system controlled by an external computer. The heating elements of on the waveguide chip are quite susceptable to heat exchange from neighbouring heating elements. While changing the voltage of the coupling region heating element of the third ring, the corresponding heating element of the fourth and second ring would get thermally influenced. The same situation can be regarded for the fifth ring influencing the fourth and sixt ring. Therefore a constant evaluation of the transmission spectrum was needed to ensure there were only the desired rings coupled in. In future experiments, it is needed consider either spending more time on redirecting all rings into the most ideal transmission spectrum. A different approach can be setting a best before measuring time, because after a certain time instance, approximately 3 minutes after setting a value on the heater, one can assume the heating elements have changed their value significantly enough compared to their original value due to the thermal exchange.

The fitting procedure could certainly improve by exploring another fitting program such as Origin. Using MATLAB provides a fast way for fitting as MATLAB already chooses some settings. The second advantage is the amount of algorithms for different situations of fitting. If boundaries are added or if special starting conditions have to be given, a case specific algorithm can be chosen. However, there is one great advantage of using Origin: it is more accurate to more digits behind the dot. This was observed by inserting the transmission spectrum of the non matching double ring resonator into Origin which resulted in an R^2 value closer to 1 than the R^2 value corresponding to the MATLAB fit. The disadvantage of Origin being that it needs a lot of starting conditons and fitting by a non standard function is slightly devious. By first fitting the data in MATLAB the starting conditions of Origin can be found. For further accuracy these fitting parameter values of MATLAB can be used as starting conditions in Origin.

Bibliography

[1] Hotta, T., Mean-field Approximation, Nanoscale Phase Separation and Colossal Magnetoresistance, Springer Series in Solid-State Sciences, Volume 136, pp 157-167

[2] Bogaerts, W. et al. (2012). Silicon microring resonators. LPR, 6 (1), 4773.

[3] Venghaus, H., Geuzebroek, Wavelength filters in fiber optics, Chapter 8, H., Driessen, A., Ring-Resonator-Based Wavelength Filters, first edition, 2006.

[4] Paloczi, G., Scheuer, J., Yariv, A.Compact Microring-Based Wavelength-Selective Inline Optical Reflector, Photonics Thechnology letters, vol. 17, no.2, 2005.

[5] Yagle, A., Z-Transforms, Their Inverses Transfer or System Functions, Fall 2005, Dept. of EECS, The University of Michigan.

[6] Chao, C., Arbor, A., Fung, W., Polymer microring resonators for biochemical sensing applications, Quantum Electronics, IEEE Journal, Volume 12, nr. 1, p. 134-142, (2006)

[7] Smith, J., Partial Fraction Expansion, Introduction to optical filter Filters with Audio Applications, online book, 2007 edition, accessed 12-8-15.

[8] Geuzebroek, H., Driessen, A., Ring-Resonator-Based Wavelength Filters, Springer Series in Optical Sciences, Volume 123, pp 341-379

[9] Vollmer, F., Fischer, P., Ring-resonator based frequency-domain optical activity measurements of a chiral liquid, Opt. Lett. 31 (2006) pp 453-455

[10] Gohring J., Dale P., Fan X., Detection of HER2 breast cancer biomarker using the opto-fluidic ring resonator biosensor, Sensors and Actuators B Volume 146, pp 226230, 2010.

[11] Curve Fitting Toolbox, Userś Guide, version 1, Chapter 3, p. 6 ,July 2001

[12] Curve Fitting Toolbox, Userś Guide, version 1, Chapter 3, p. 14 ,July 2001

[13] Rafizadeh, D., Zhang, J., Tiberio, R., Ho, S., Propagation Loss Measurements in Semiconductor Microcavity Ring and Disk Resonators, Journal of lightwave technology, vol. 16, no. 7, July 1998.

[14] Wang, J., Loss, Reflection and Transmission Measurement and Analysis of Silicon-on-Insulator Ring Resonator, University of Pennsylvania, NNIN REU 2006.

[15] McKinnon, W., Xu, D., Storey, C., Post, E., Densmore, A., Delage, A., Wladron, P., Schmid, J., Janz, S., Extracting coupling and loss coefficients form a ring resonator, Optics Express, Vol. 17, No. 21, October 2009.

[16] Geuzebroek, H., Driessen, A., Ring Resonator-Based Wavelength Filters.